Iron weathering products in a CO2+(H2O or H2O2) atmosphere: Implications for weathering processes on the surface of Mars

V. F. Chevrier, P.- E. Mathé, P. Rochette, O. Grauby, Guilhem Bourrié, Fabienne Trolard

Available online at www.sciencedirect.com
ScienceDirect
Geochimica et Cosmochimica Acta 70 (2006) 4295–4317
Geochimica
www.elsevier.com/locate/gca

Iron weathering products in a $CO_2 + (H_2O$ or $H_2O_2)$ atmosphere: Implications for weathering processes on the surface of Mars

V. Chevrier [a,*], P.-E. Mathé [b], P. Rochette [b], O. Grauby [c], G. Bourrié [d], F. Trolard [d]

[a] *W. M. Keck Laboratory for Space Simulation, Arkansas Center for Space and Planetary Sciences, Muse 202, University of Arkansas, Fayetteville, AR 72701, USA*
[b] *Centre Européen de Recherche et d'Enseignement en Géosciences de l'Environnement, Europôle de l'Arbois, BP 80, 13545 Aix-en-Provence, Cedex 04, France*
[c] *Centre de Recherche en Matière Condensée et Nanosciences, Centre National de la Recherche Scientifique, Campus de Luminy, case 913, 13288 Marseille, Cedex 13, France*
[d] *Institut National de Recherche Agronomique, Europe de l'Arbois, BP 80, 13545 Aix-en-Provence, Cedex 04, France*

Received 8 March 2005; accepted in revised form 16 June 2006

Abstract

Various iron-bearing primary phases and rocks have been weathered experimentally to simulate possible present and past weathering processes occurring on Mars. We used magnetite, monoclinic and hexagonal pyrrhotites, and metallic iron as it is suggested that meteoritic input to the martian surface may account for an important source of reduced iron. The phases were weathered in two different atmospheres: one composed of $CO_2 + H_2O$, to model the present and primary martian atmosphere, and a $CO_2 + H_2O + H_2O_2$ atmosphere to simulate the effect of strong oxidizing agents. Experiments were conducted at room temperature and a pressure of 0.75 atm. Magnetite is the only stable phase in the experiments and is thus likely to be released on the surface of Mars from primary rocks during weathering processes. Siderite, elemental sulfur, ferrous sulfates and ferric (oxy)hydroxides (goethite and lepidocrocite) are the main products in a water-bearing atmosphere, depending on the substrate. In the peroxide atmosphere, weathering products are dominated by ferric sulfates and goethite. A kinetic model was then developed for iron weathering in a water atmosphere, using the shrinking core model (SCM). This model includes competition between chemical reaction and diffusion of reactants through porous layers of secondary products. The results indicate that for short time scales, the mechanism is dominated by a chemical reaction with second order kinetics ($k = 7.75 \times 10^{-5}$ g^{-1}/h), whereas for longer time scales, the mechanism is diffusion-controlled ($De_A = 2.71 \times 10^{-10}$ m^2/h). The results indicate that a primary CO_2- and H_2O-rich atmosphere should favour sulfur, ferrous phases such as siderite or Fe^{2+}-sulfates, associated with ferric (oxy)hydroxides (goethite and lepidocrocite). Further evolution to more oxidizing conditions may have forced these precursors to evolve into ferric sulfates and goethite/hematite.

1. Introduction

This paper extends previous work on experimental weathering under martian conditions (Chevrier et al., 2004). In situ observations made by the various landers on Mars have shown the association of colored iron (oxy)hydroxides (Morris et al., 2000), detected by remote sensing with strongly magnetic phase(s) of an unknown nature (Hargraves et al., 1979; Hviid et al., 1997; Bertelsen et al., 2004), possibly maghemite γ-Fe_2O_3 (Hargraves et al., 2000) and/or (titano)magnetite $Fe_{3-x}Ti_xO_4$ (Gunnlaugsson et al., 2002; Goetz et al., 2005). The nature of the iron (oxy)hydroxide(s) also remains a subject of debate, but the reflectance spectra of the martian surface appears to be most consistent with hematite (Morris et al., 1989) or goethite (Morris and Golden, 1998). Hematite is also the

* Corresponding author.
E-mail address: vchevrie@uark.edu (V. Chevrier).

0016-7037/$ - see front matter © 2006 Elsevier Inc. All rights reserved.
doi:10.1016/j.gca.2006.06.1368

only thermodynamically stable iron oxide in the present-day conditions of the surface of Mars (Gooding, 1978). The large formations of "grey crystalline hematite" discovered by Mars Odyssey (Christensen et al., 2000; Hynek et al., 2002) have various possible origins, including precipitation from a low-temperature aqueous phase, burial or thermal metamorphism favoured by hydrothermalism, deuteritic alteration of lava, weathering processes etc. (Christensen et al., 2001; Catling and Moore, 2003; Baldridge and Calvin, 2004; Christensen and Ruff, 2004). Mars Exploration Rover (MER) Opportunity has provided evidence for the past presence of water in Meridiani Planum (Squyres et al., 2004) by the observation of sedimentary layers containing jarosite ($(H_3O^+, K^+)Fe^{3+}_3(SO_4)_2(OH)_6$) and spherical aggregates of crystalline hematite, so called "blueberries" (Klingelhöfer et al., 2004). Several studies have suggested the possibility for early aqueous alteration, when Mars was covered by a dense atmosphere, and temperatures supported liquid water (Burns, 1993; Catling, 1999). Alternatively, rapid alteration during catastrophic release of water on the surface may be sufficient to account for some geochemical and mineralogical observations on Mars (Madden et al., 2004).

Viking, Pathfinder and MER Spirit observations suggest that surface alteration processes remained relatively limited (Haskin et al., 2005). Some arguments supporting this hypothesis are the presence on the surface of minerals highly sensitive to oxidation/alteration processes like olivine (Christensen et al., 2003), or magnetite (Goetz et al., 2005). However weathering in present cold and dry conditions has been suggested, resulting the formation of poorly crystalline phases (Banin et al., 1993; Banin, 1996). Finally, gas–solid alteration process may be effective today because of the lack of available liquid water, and the good correspondence between predicted mineralogy and observations (Gooding, 1978). Such recent alteration products could cover and/or be mixed with early-water driven alteration assemblages, complicating the distinction between successive periods of martian history (Banin, 1996).

Despite their apparent complexity, the various mineralogical, chemical and morphological features of the martian surface point toward weathering as the main global process responsible for its evolution. This assumption is strengthened by the similarity between terrestrial red soils and the martian regolith, both containing frequent association between red-colored fully oxidized iron-bearing phases (hematite and goethite) and magnetic spinel (Allan et al., 1988; Goulart et al., 1998).

Therefore, we performed weathering experiments in order to test two main factors regarding the formation and evolution of the martian regolith: the primary substrate and the atmosphere. As magnetic properties have been extensively used to investigate the martian surface, we decided to explore the alteration behaviour of the strongly magnetic primary phases magnetite Fe_3O_4, pyrrhotite $Fe_{1-x}S$ and pure elemental iron. Pyrrhotite was used because several studies have shown that the main magnetic carrier in SNC meteorites is pyrrhotite rather than magnetite (Rochette et al., 2001). SNC meteorites are also about 2–3 times enriched in sulfides compared to their terrestrial equivalents (Lorand et al., 2005). In addition, the similarity between martian surface petrology and sulfide-rich komatiitic formations on Earth suggest that sulfates observed on Mars are the result of the interaction between silicate bedrock and sulfide deposits during weathering (Burns and Fisher, 1990; Burns and Fisher, 1993). Therefore, it seems likely that sulfides could play an important role in the evolution of the martian surface.

Finally, we studied the behaviour of pure metallic iron. A billion years of meteorite bombardment on the surface of Mars (and the lack of any tectonic activity), provides an important source of metallic iron, observed recently on Mars by MER Opportunity (http://marsrovers.jpl.nasa.gov/newsroom/pressreleases/20050119a.html). Various models have estimated the meteoritic contribution, including interplanetary dust particles, leading to a range from a few wt% to nearly 30 wt% of the regolith (Flynn and McKay, 1990; Bland and Smith, 2000). Meteorites are generally enriched in Ni-bearing iron metal, and sulfides, mainly troilite, FeS. Ni enrichments observed in Gusev Crater from fresh, abraded surfaces of Adirondack rock, altered surfaces and regolith (Gellert et al., 2004) are consistent with the contribution of a Ni rich source, most likely meteoritic (Yen et al., 2005).

During our experiments we used two types of atmospheres: one composed of CO_2 and H_2O, and the second of CO_2, H_2O and hydrogen peroxide, H_2O_2. The aim of the first atmosphere was to study weathering under current martian atmospheric conditions, i.e. dominated by CO_2 (95.3% of the martian atmosphere) and with nearly no O_2 (0.13% of the martian atmosphere). Moreover, the use in our experimental conditions of high CO_2 pressure (0.75 atm) at relatively high temperature (15–20 °C), in addition to the need to observe significant alteration, allowed us to study weathering in a possible primary CO_2 and H_2O-rich atmosphere. A dense atmosphere may have been present in the early history of Mars, due to abundant volcanic outgassing, that resulted in an important greenhouse effect (Pollack et al., 1987; Forget and Pierrehumbert, 1997; Phillips et al., 2001). We used H_2O_2 in the second atmosphere because recent observations show that this molecule is present in the martian atmosphere (Clancy et al., 2004; Encrenaz et al., 2004) with a column density of about 10^{15}–10^{16} cm^{-2}. In addition, Viking biological experiments suggest that other strongly oxidizing species produced by photochemistry in the martian atmosphere could interact with the regolith (Oyama et al., 1978; Yen et al., 2000).

2. Methods

2.1. Sample descriptions

Five different samples have been used for this study, including four minerals and one mixture of two phases.

The minerals are: synthetic magnetite Fe_3O_4 (PROLABO product number 24187.291), synthetic elemental iron α-Fe (MERCK product number 1.03819.0100), natural hexagonal pyrrhotite HPo $Fe_{0.9}S$ from Ducktown Mine, Tennessee, USA (Carpenter, 1974) and natural monoclinic pyrrhotite MPo of unknown origin, provided by the Museum d'Histoire Naturelle de Paris. Both pyrrhotites have been prepared by manually grinding the samples in an agate mortar. The grain size range was 1–10 μm for α-Fe, 1-25 μm for magnetite and 5–100 μm for pyrrhotites. The broad grain size for pyrrhotite is representative of the usual grain size of sulfides and in basaltic rocks while the grain size of elemental iron is close to IDP's average size of a few to a few tens of micrometers. The mixture was composed of 50 wt% α-Fe and 50 wt% MPo. The mineralogy and composition of both pyrrhotites have been verified by X-ray diffraction (XRD), thermomagnetic curves, scanning electron microscopy (SEM) and transmission electron microscopy (TEM). MPo contains about 7.5% pentlandite $(Fe_{0.56}Ni_{0.44})_9S_8$. HPo contains about 5% chalcopyrite and about 0.5 wt% monoclinic pyrrhotite. Finally both pyrrhotites contain traces of silicates: biotite and actinolite in HPo, biotite in MPo.

2.2. Experimental protocol

All natural samples have been powdered and the grain size verified by SEM observations. Ten grams of each sample was poured in a glass cup and then placed in a dessicator. The first dessicator was filled with 1 L of pure deionized liquid water and the second with 1 L of liquid water containing 33% hydrogen peroxide H_2O_2. We purged the atmosphere from the dessicators and replaced it by 0.75 atm (56 cm Hg) of gaseous CO_2. This step has been done twice to obtain an initial atmosphere composed of 99% CO_2. We used water equilibrated with the Earth atmosphere and thus containing amounts of dissolved O_2 (about 10 mg/L in the experimental conditions). We used two dessicators for sampling at different times (one per atmosphere), and two control dessicators with the same atmospheres which remained closed during the whole experiment, in order to check the possible perturbation due to contact with terrestrial atmosphere, i.e. with oxygen, when opening. The control dessicators being smaller than the sampling dessicators, they were filled with 0.5 L of liquid and the mass of powder was 5 g. The equilibration between liquid water and gaseous CO_2 is relatively fast (a few hours) and thus does not significantly affect the weathering kinetics, which are much slower. The temperature remained in the range 15–20 °C. Before sampling the material was mixed in the cup, to separate the grains and homogenize the products. At each step we sampled between 0.5 and 1.0 g of material for analysis. Sampling and analyses ware carried out as fast as possible to avoid any equilibration with the Earth atmosphere. Nevertheless, we checked this possible effect by exposing some samples to air for 1 month. No change in composition or structure has been observed. Thus, we considered that the main chemical and mineralogical changes occurred in the dessicators. Finally, experiments have been conducted in near complete darkness, to avoid destabilization of hydrogen peroxide by light. Due to the very slow reaction kinetics, sampling was performed at 5, 19, 40, 75, 117, 173, 259, 411 and 520 days. The mixture (MPo + α-Fe) was sampled at 21, 56, 98, 154, 240, 392 and 501 days. Finally control powders were sampled at 490 days (or d in the rest of the text).

2.3. Analytical methods

Combined mineralogical and rock magnetic analyses were used to characterize the evolution of primary phases as well as the nature and structure of the reaction products. Systematic measurements of saturation magnetization M_S were done using a P.M.C. VSM micromagnetometer Model 3900 in CEREGE. Hysteresis cycles were done with a 1 T maximum field and a step of 10 mT. Low field magnetic susceptibility χ_{LF} versus temperature curves have been done in the range 20–700 °C using an AGICO Kappabridge KLY2 coupled to a CS2 system in CEREGE, and a Kappabridge KLY3 coupled to a CS3 system in St. Maur. χ_{LF} versus temperature curves have been obtained under an argon flow to avoid oxidation effects.

X-ray powder diffraction patterns have been recorded on a Philips PW 3710 $\theta/2\theta$ diffractometer using $Co_{K\alpha}$ ($\lambda = 1.79$ Å) radiation with a secondary flat graphite monochromator. The diffractometer optics used to record all samples was a front fixed slit of 1°, a scattered-radiation slit of 1° after the sample and a detector slit of 0.2 mm. The X-ray tube operating conditions were 35 kV and 30 mA. The 2θ range was 5–80° in 0.02° steps and a counting time of 12 s (12.5 h of total counting). All powder samples were displayed on a cut silicon plate (no Bragg peaks) and homogenized with alcohol to obtain a thin and very homogeneous layer. Scanning electron microscopy (SEM) observations have been performed using a Philips XL 30 ESEM (St. Charles Faculty, Marseille, France) coupled with an EDX analytical system (EDAX) for semi-quantitative chemical analyses. Additional pictures of control samples were acquired with a Hitachi S-3000 working with an accelerating voltage of 3.5 kV. For transmission electron microscopy (TEM) observations, powders were dispersed quickly in alcohol and settle down on a carbon-coated Cu grid. TEM images and low-energy electron diffraction patterns of specific phases were carried out with a JEOL—2000 FX (CRMCN, Marseille), operating with a beam intensity of 126 mA and an accelerating voltage of 200 kV. Microanalyses were acquired with a Si(Li) detector fitted with a UTW and a TRACOR Northern 5500 EDS system. In fixed transmission mode, the spot size diameter ranged from 40 to 100 nm. Quantitative data were obtained by the method developed by Cliff and Lorimer (1975) after calibration of the $k_{x,Si}$ factors (x = Al, Mg, ...) against natural and synthetic layer silicates of known and homogeneous composition.

3. Results

The saturation magnetization M_S of weathered products is presented in Table 1. A summary of the weathering product phases is presented in Table 2. M_S values of highly magnetic primary phases α-Fe, magnetite, MPo and the mixture (α-Fe + MPo) are several orders of magnitude higher than the associated weathering products (carbonates, sulfur, sulfates and iron (oxy)hydroxides, see below). Therefore, M_S is proportional to the mass fraction of the residual primary phase and is presented in the figures as percentages of initial values.

3.1. Magnetite

Magnetite does not show any change during the whole experiment, whatever the atmosphere used.

3.2. Elemental iron

According to X-ray diffraction and magnetic measurements, α-Fe remains unchanged in the peroxide atmosphere, whereas it undergoes significant reaction in the water-bearing atmosphere. The evolution of M_S indicates that 75% of the initial mass has been converted into secondary products between 0 and 259 days (Fig. 1), and the remaining mass does not change further with time. The secondary phases identified by XRD are siderite ($FeCO_3$) and goethite (α-FeOOH, Fig. 2). Siderite appears on iron particles after 19 d, forming small rhombohedral crystals observed with SEM (Fig. 3A). Etch pits observed by SEM on siderite crystals (Fig. 3B) prove its instability in the experimental conditions. The presence of a ferrihydrite-type phase, previously inferred from TEM observations (Chevrier et al., 2004), has been confirmed by X-ray diffraction (Fig. 4). Comparison of the background of XRD patterns (obtained by subtracting the peaks of identified phases, i.e. iron, siderite and goethite) shows a very flat background at $t = 40$ d (containing almost only siderite), whereas the XRD pattern at $t = 75$ d is similar to the pattern of ferrihydrite synthesized using the method of Schwertmann and Cornell (1991). The evolution with time from ferrihydrite to goethite is also verified on XRD patterns that show a marked decrease of the area of the main peak of goethite ($d_{101} \sim 4.19$ Å or $2\theta \sim 24.65°$) normalized to its intensity (Fig. 5). This parameter gives a specific angle (and thus a specific domain size) characteristic of the degree of crystallinity of goethite, more accurate than the usual parameter used, i.e. the full width at half maximum or FWHM.

3.3. Pyrrhotites

According to XRD (Figs. 6 and 7), SEM (Fig. 8) and TEM (Fig. 9), both pyrrhotites alter to similar reaction products in both atmospheres, i.e. elemental sulfur, goethite and sulfates (Fig. 9A). In the water atmosphere, goethite forms small crystallites, under 200 nm in size (Figs. 8A, 9A and B), associated with an amorphous iron

Table 1
Saturation magnetization M_S in A.m^2/kg of aged products and control samples

t (days)	α-Fe	Magnetite	MPo	HPo	t (days)	α-Fe + MPo
($CO_2 + H_2O$) atmosphere						
0	210.0	89.0	11.79	10.31×10^{-2}	0	133.9
5	213.1	85.4	12.72	6.52×10^{-2}	21	75.5
19	215.1	85.0	10.91	6.87×10^{-2}	56	55.3
40	157.0	90.4	11.14	5.63×10^{-2}	98	41.4
75	105.0	85.6	10.12	7.73×10^{-2}	154	26.9
117	85.4	93.6	8.63	17.98×10^{-2}	240	14.2
173	67.6	85.3	8.43	32.30×10^{-2}	392	12.3
259	49.0	85.0	8.14	55.36×10^{-2}	501	10.5
411	52.5	83.1	3.77	9.15×10^{-2}		
520	52.5	n.d.	1.53	0.97×10^{-2}		
Control	127.7	n.d.	3.58	10.20×10^{-2}		
($CO_2 + H_2O + H_2O_2$) atmosphere						
0	210.0	89.0	11.79	10.31×10^{-2}	0	133.9
5	224.6	93.7	12.77	8.27×10^{-2}	21	110.4
19	229.3	85.3	12.29	7.18×10^{-2}	56	113.9
40	215.7	87.5	11.39	6.82×10^{-2}	98	90.1
75	254.0	91.2	10.19	7.40×10^{-2}	154	70.0
117	194.2	85.4	9.49	5.96×10^{-2}	240	62.5
173	207.1	88.3	9.07	6.82×10^{-2}	392	50.7
259	265.0	85.8	8.30	7.14×10^{-2}	501	45.7
411	211.3	87.7	8.19	7.51×10^{-2}		
520	n.d.	n.d.	7.42	11.85×10^{-2}		
Control	n.d.	n.d.	7.99	13.60×10^{-2}		

n.d., not determined.

Table 2
Summary of neoformed phases during experimental weathering of MPo, HPo and α-Fe

Atmosphere	Water ($H_2O + CO_2$)			Hydrogen peroxide ($H_2O + H_2O_2 + CO_2$)	
	α-Fe	MPo	HPo	MPo	Hpo
	Siderite[a] Goethite Ferrihydrite[a] Magnetite[a]	Sulfur Goethite Ferrihydrite[a] Melanterite Rozenite Gypsum	Sulfur Ferrihydrite[a] Goethite Melanterite Gypsum	Sulfur Goethite Melanterite[a] Jarosite	Sulfur Goethite Jarosite Coquimbite mpo[b]
Control samples					
Atmosphere	($H_2O + CO_2$)			($H_2O + H_2O_2 + CO_2$)	
	α-Fe	MPo	HPo	MPo	Hpo
	Goethite	Goethite Lepidocrocite Sulfur Melanterite	Goethite Lepidocrocite Sulfur	Jarosite Copiapite Coquimbite Butlerite Melanterite Sulfur Goethite	Jarosite Copiapite Coquimbite Butlerite Sulfur Goethite

Only the phases strictly identified have been presented in this table. However, ferrihydrite has been systematically observed associated to goethite in products studied with TEM and X-ray diffraction. Its presence is then very likely in all goethite-containing products. Formulas: butlerite: $Fe^{3+}(SO_4)(OH).2H_2O$; copiapite: $Fe^{2+}Fe^{3+}{}_4(SO_4)_6(OH)_2.20H_2O$; coquimbite: $Fe^{3+}{}_2(SO_4)_3{\cdot}9H_2O$; ferrihydrite: $5Fe_2O_3{\cdot}9H_2O$; goethite: α-FeO(OH); gypsum: $CaSO_4{\cdot}2H_2O$; jarosite: $KFe^{3+}{}_3(SO_4)_2(OH)_6$; lepidocrocite: γ-FeO(OH); melanterite: $FeSO_4{\cdot}7H_2O$; rozenite: $FeSO_4{\cdot}4H_2O$; siderite: $FeCO_3$; sulfur: S.
[a] Metastable phases at the time scale of experiments.
[b] Monoclinic pyrrhotite Fe_7S_8.

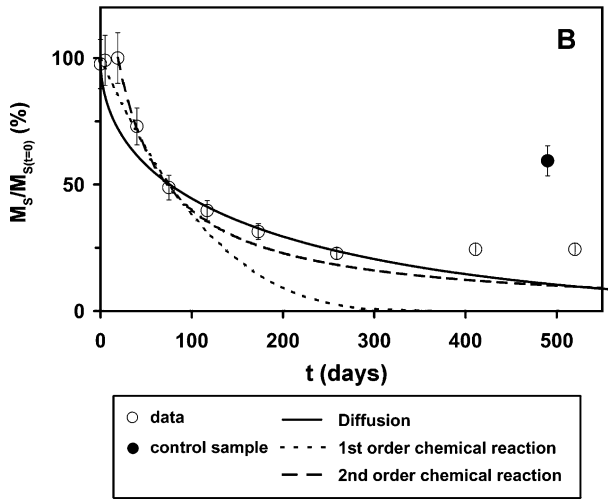

Fig. 1. Evolution with time of normalized saturation magnetization M_S of α-Fe weathered in water atmosphere. The fitting curves correspond to application of the kinetic shrinking core model (SCM) described in Section 4.3.

(oxy)hydroxide. Elemental sulfur is the dominant S-bearing phase in the water atmosphere (Figs. 6 and 7), forming rounded crystals (Fig. 8B). Melanterite ($FeSO_4{\cdot}7H_2O$, Fig. 8C), and sometimes rozenite ($FeSO_4{\cdot}4H_2O$) are the only iron sulfate detected in pyrrhotites weathered in the water atmosphere, and develop mainly in MPo. Finally, small amounts of gypsum ($CaSO_4{\cdot}2H_2O$) have been detected in HPo (Figs. 8B and 9A).

In the peroxide atmosphere, sulfur is less abundant than in the water atmosphere, and presents various morphologies, from well-formed rounded crystals (Fig. 8D) to small filaments (Fig. 9C). These filaments are composed of thin, elongated crystals, around 100 nm long (Fig. 9D). Sulfur is closely associated to goethite which forms crusts without visible crystals (Fig. 8E). The sulfate assemblage observed in the peroxide atmosphere is different and includes minor melanterite (at 259 d in MPo) and minor Fe^{3+}-sulfates, i.e. jarosite $(K^+, Na^+, H_3O^+)Fe^{3+}{}_3(SO_4)_2(OH)_6$ identified by SEM and TEM (Figs. 8F and 9E) and other ferric sulfates. By analogy with observations on control samples (see below) and observations of morphologies, these accessory sulfates are probably copiapite $Fe^{2+}Fe^{3+}{}_4(SO_4)_6(OH)_2 \cdot 20H_2O$ forming aggregates of thin plates (Fig. 8G), coquimbite $Fe^{3+}{}_2(SO_4)_3 \cdot 9H_2O$ presenting thicker crystals (Fig. 8H) and butlerite/parabutlerite $Fe^{3+}(SO_4)(OH){\cdot}2H_2O$ as isolated elongated tabular crystals (Fig. 8H). Coquimbite has also been characterized by TEM observation and diffraction pattern (Fig. 9F).

The M_S profile of MPo is similar in both atmospheres from 0 to 259 d, presenting a diminution of about 30% (Fig. 10A). Between 259 and 520 d, M_S does not evolve any more in the peroxide atmosphere, whereas it strongly decreases in the water atmosphere, down to 70% of the initial M_S. Both results indicate replacement of ferrimagnetic MPo by secondary weakly magnetic phases. If the weathering process starts rapidly in the peroxide atmosphere, with formation of secondary crusts after only 5 d, the cumulated transformation after 520 d is actually larger in the water atmosphere.

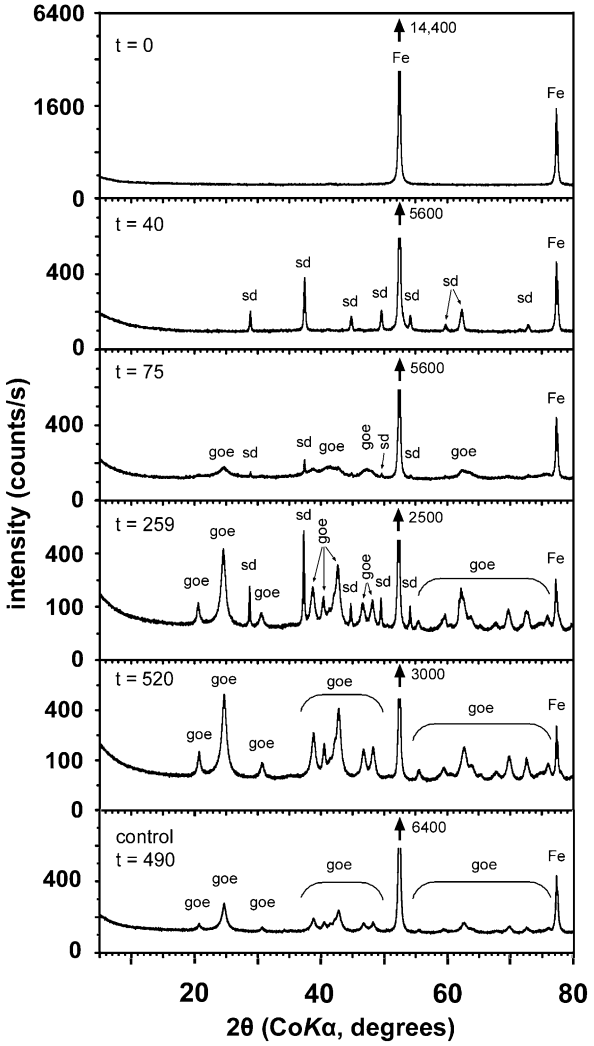

Fig. 2. X-ray diffractograms of α-Fe at different steps of weathering in water atmosphere, respectively $t = 0$, 40, 75, 259, 520 days and the control sample ($t = 490$ days). For more clarity the main peak of α-Fe has been truncated. The numbers beside the arrows are the maximum intensity of the α-Fe main peak. *Abbreviations:* Fe, α-Fe; sd, siderite; goe, goethite.

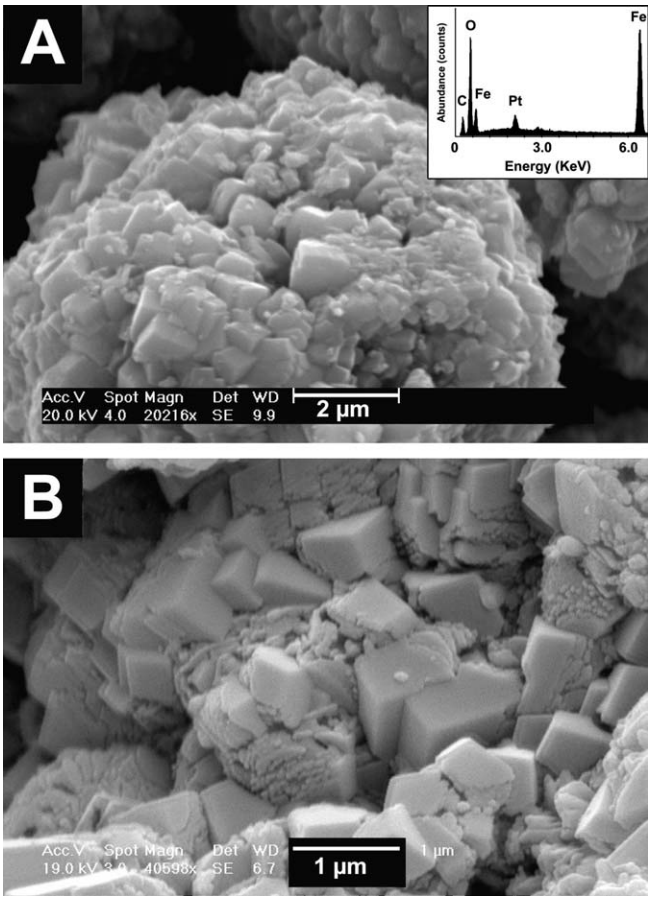

Fig. 3. SEM pictures of neoformed products on α-Fe particles weathered in water atmosphere. (A) Rhombohedral crystals of siderite ($t = 40$ days). (B) Corrosion and dissolution features on siderite crystals ($t = 259$ days).

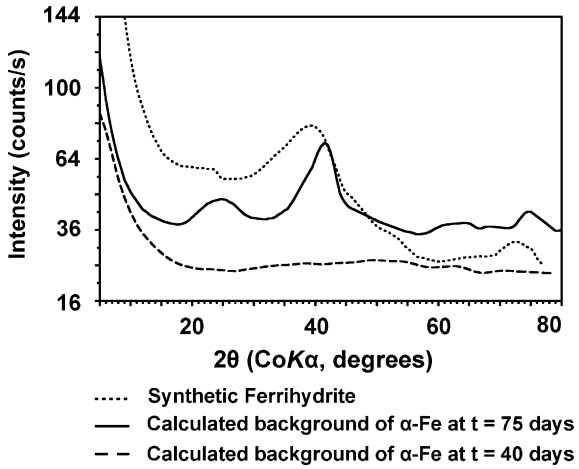

Fig. 4. X-ray diffraction calculated background of α-Fe weathered at $t = 40$ d and at $t = 75$ d. Comparison with the spectrum of an artificial ferrihydrite-2 L obtained by the method of Cornell and Schwertmann (1991).

The M_S profile of HPo in water atmosphere shows a linear increase between 75 and 259 d (Fig. 10B) followed by a strong decrease of both parameters between 259 and 411 d. This increase represents about five times the initial M_S value indicating the neoformation of a ferri/ferromagnetic phase. On the χ_{LF} versus temperature curves, HPo is identified by two transitions: the first at 220 °C corresponds to the γ-transition (Fig. 11), i.e. the transformation of antiferrromagnetic HPo into ferrimagnetic HPo (Dekkers, 1988). The second transition is the Curie temperature of ferrimagnetic HPo at 295 °C (Fig. 11). A third transition at 320 °C corresponds to the Curie temperature of traces of monoclinic pyrrhotite in the HPo sample (Carpenter, 1974). However, the intensity of the Curie transition is very weak at $t = 0$ (Fig. 11), and increases progressively with time, reaching a maximum at $t = 259$ d (Fig. 11). Then a neoformed transient monoclinic pyrrhotite is directly responsible for the increase of M_S with time. The main M_S value for pure monoclinic pyrrhotite is 15 Am^2/kg giving about 0.5–1 wt% monoclinic pyrrhotite at $t = 0$ and 3–3.5 wt% at $t = 259$ d. Monoclinic pyrrhotite is also neoformed in peroxide atmosphere but the signal remains very weak compared to the water atmosphere.

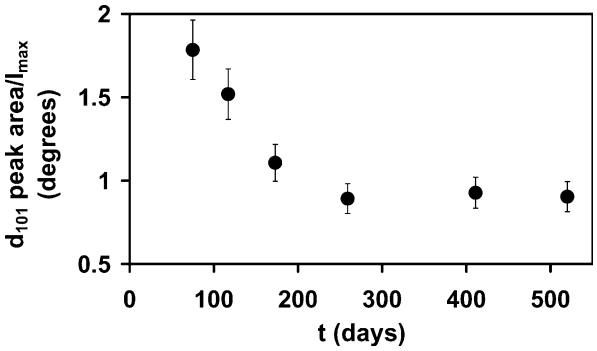

Fig. 5. Area of the d_{101} peak of goethite formed on weathered α-Fe, normalized to its peak height, as a function of time.

3.4. Mixture of MPo and α-Fe

The secondary mineralogy in the mixture (MPo + α-Fe) is similar to the product mineralogy from separate phases. Goethite, sulfur and sulfates are formed in the peroxide atmosphere, whereas goethite, siderite, and small amounts of sulfur and sulfates are formed in the water atmosphere. Compared to pure α-Fe in the water atmosphere, siderite represents only a small fraction of the secondary phases. Siderite is also a metastable phase, as no signal is detected on X-ray diffraction patterns after 240 d.

M_S of (MPo + α-Fe) decreases strongly with time. At 392 d, M_S value is about 10% of the initial value in the water atmosphere (Fig. 12) and 40% in the peroxide atmosphere (Fig. 12). Considering our mixture of 50 wt% α-Fe and 50 wt% MPo, and the M_S values of separate phases, i.e. 215 Am^2/kg for α-Fe and 15 Am^2/kg for MPo, the average M_S of (α-Fe + MPo) is 115 Am^2/kg. Thus, at $t = 0$, the α-Fe accounts for 93% of the M_S value while the MPo accounts only for 7%. Therefore the 40% decrease of M_S in the peroxide atmosphere implies that α-Fe is weathered with the MPo. This corresponds to 33–40 wt% α-Fe weathered, depending on the mass of MPo weathered (100 wt% MPo weathered corresponds to a loss of 7% of the M_S signal and then to a minimal loss of α-Fe of 33 wt%). Therefore, α-Fe remains unaltered in the peroxide atmosphere, and is weathered if mixed with MPo.

3.5. Control samples (490 days of weathering)

α-Fe is not weathered in the peroxide atmosphere. In the water atmosphere, weathering of the α-Fe appears to cease earlier compared to the other water dessicator. M_S measurement shows that only 40 wt% α-Fe has been transformed (Fig. 1) compared to 75 % at 520 d for the powders sampled during ageing. Goethite is the only observed neoformed phase (Fig. 2).

MPo and HPo are weathered in a similar rate to their equivalent in the sampled dessicators (Fig. 10) with the same secondary assemblages (Figs. 13 and 14) including elemental sulfur (Fig. 15A), Fe^{2+}-sulfates and iron (oxy)hydroxides (Fig. 15B) in the water atmosphere, and Fe^{3+}-sulfates in the peroxide atmosphere (Fig. 15C and D). One notable difference in the water atmosphere is the presence of lepidocrocite γ-FeOOH in similar content to goethite in both pyrrhotites (Figs. 13A, 14A,Fig. 15B). Furthermore, substantial amounts of melanterite are present in the MPo sample (Fig. 13A), but not in HPo. In the peroxide atmosphere, the alteration profile is quite different, with a 1-mm thick crust of loose neoformed products (surface crust) covering a layer of relatively unaltered material (“fresh” underlying layer). Both layers were manually separated for analysis. The “fresh” layer shows mainly relatively intact pyrrhotite, with small amounts of neoformed goethite and elemental sulfur (Figs. 13B and 14B). The crust is composed of a complex assemblage of Fe^{3+}-sulfates including jarosite, copiapite, coquimbite and minor butlerite (Figs. 13C and 14C). In the HPo sample, jarosite is the dominant sulfate (Figs. 13C and 15C), whereas copiapite and jarosite dominate in MPo (Figs. 14C and 15D).

All powders, i.e. α-Fe, HPo and MPo, weathered in the water atmosphere are completely cemented by neoformed phases, suggesting that water has percolated through the powders. We have measured the water content of the control samples by comparing their mass just after removal from the experimental atmosphere, and after 24 h of dessiccation in an Ar atmosphere. For the samples weathered in the water atmosphere, MPo presents a higher water content (15.4 ± 0.1 wt%) than HPo (5.5 ± 0.1 wt%) and α-Fe (0.3 ± 0.1 wt%). Control samples of pyrrhotite weathered in the peroxide atmosphere do not show any absorbed water, and grains are not cemented by neoformed phases.

4. Weathering mechanisms

An important point that must be highlighted before any interpretation regarding our results concerns the effect of free oxygen O_2, which is a strong oxidant and may influence the weathering mechanism (Filippou et al., 1997; Janzen et al., 2000; Mikhlin et al., 2002). The amount of dissolved O_2 at 15–20 °C and 0.75 atm is 6.6–7.4 mg/L. Considering only iron weathering; a maximum of 40 wt% of the initial 5 g α-Fe has been converted into goethite at the end of the experiment in the control sample. This represents 2 g of goethite FeO(OH), and 1.14 g of O_2. Supposing that all the O_2 dissolved in water (~3.5 mg in 0.5 L) has reacted to form goethite, this represents a maximum of 0.3 wt% of the oxygen used for the reactions. This implies that the dissolved oxygen contribution to the weathering process is almost negligible, particularly since MPo and HPo react also with O_2. In addition, the solubility of oxygen decreases by 10–20% in solutions containing high (0.5–1 M) sulfate or sulphuric acid (Kaskiala, 2002; Jerz and Rimstidt, 2004). The opening of the dessicators, when sampling, could have allowed the water to reequilibrate with the terrestrial atmosphere. Therefore, the total amount of O_2 is more important than in the control dessicators which remained closed during the whole experiment. With the assumption that all the O_2 dissolved in water was complete-

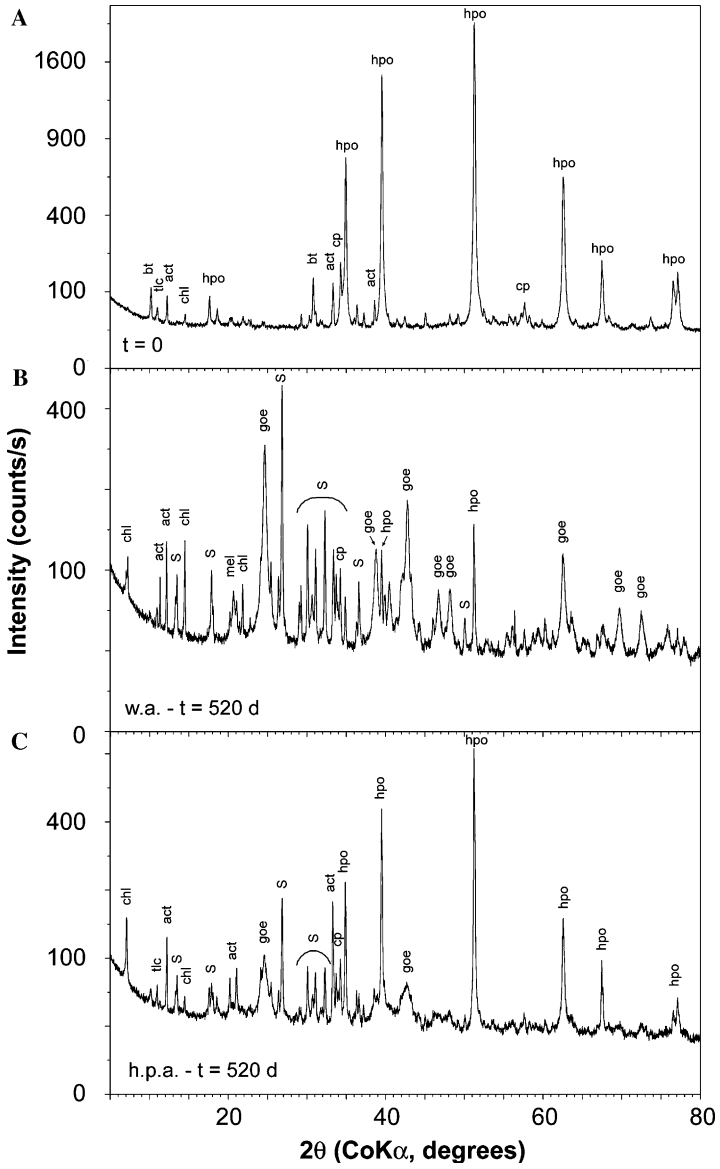

Fig. 6. X-ray diffraction patterns of hexagonal pyrrhotite (HPo). (A) $t = 0$, (B) after 520 days in the water atmosphere (w.a.), (C) after 520 days in the peroxide atmosphere (h.p.a.). *Abbreviations:* act, actinolite; bt, biotite; chl, chlorite; cp, chalcopyrite; goe, goethite; hpo, hexagonal pyrrhotite; mel, melanterite; S, elemental sulfur; tlc, talc.

ly used by the chemical reactions and then fully recharged during the opening of the dessicators, this leads to a maximum of ~3.7 wt% O_2 used for the formation of goethite in the iron. Therefore, in the rest of the discussion we will consider the major processes as occurring without O_2, even though some minor effects are possible.

In our experiments the water does not represent an overabundant phase compared to other species, so we have not been able to determine the concentrations of dissolved species. Therefore determination of mechanisms is based on mineralogical observations of secondary phases. Nevertheless, as the mechanisms are similar to capillary condensation at water saturation, we make the reasonable assumption that water chemical activity is 1. The chemical pathways used to explain our results, are described in the following paragraphs, and summarized in Fig. 16.

4.1. Elemental iron α-Fe

Considering the minor role played by dissolved O_2 in our experiments, the main oxidant here is rather the redox couple H^+/H_2, or directly water (H_2O/H_2), promoted by the dissolution of CO_2. The pH of the main solution of 3.95, measured at the end of the experiments in the remaining liquid water in the control dessicators, and in good accordance with the calculated value of 3.92 for a solution in equilibrium with a CO_2 atmosphere at 0.75 atm. Thus the initial reaction of α-Fe weathering is:

$$Fe^0_{(s)} + H_2O_{(l)} + CO_{2(aq)} = FeCO_{3(s)} + H_{2(g)} \quad (1)$$

The Gibbs free energy of the reaction is $\Delta_R G°$ (10^5 Pa, 298.15 K) = −43.58 kJ/mol, which indicates that the reac-

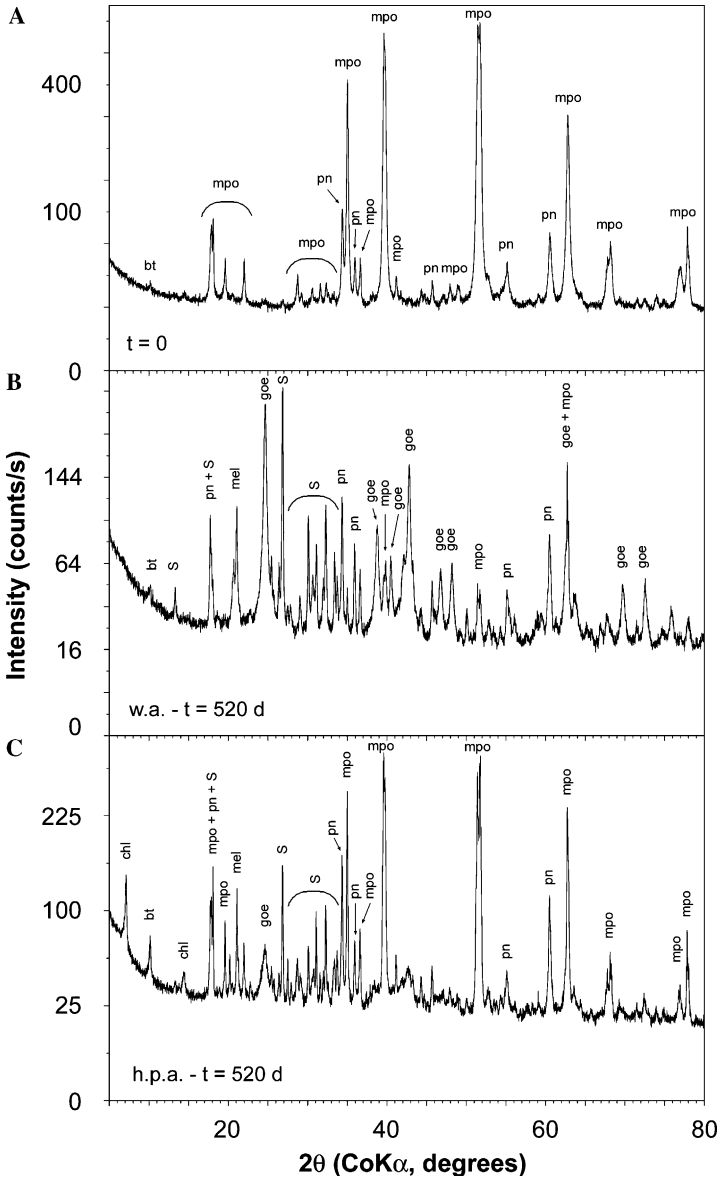

Fig. 7. X-ray diffraction patterns of monoclinic pyrrhotite (MPo). (A) $t = 0$, (B) after 520 days in the water atmosphere (w.a.), (C) after 520 days in the peroxide atmosphere (h.p.a.). *Abbreviations:* bt, biotite; chl, chlorite; goe, goethite; mel, melanterite; mpo, monoclinic pyrrhotite; pn, pentlandite; S, elemental sulfur.

tion is favoured toward siderite formation. Previous studies on iron in bicarbonate solution and anoxic conditions ($O_2 < 2$ ppm compared to our <4 wt%) have shown the formation of siderite and iron (oxy)hydroxides (Savoye et al., 2001). In the absence of O_2, the formation of goethite in only possible via the following reaction implying transformation of siderite:

$$FeCO_{3(s)} + H_2O = \alpha\text{-}FeO(OH)_{(s)} + \tfrac{1}{2}H_{2(g)} + CO_{2(aq)} \quad (2)$$

The Gibbs free energy of this reaction is positive, i.e. $\Delta_R G^\circ$ (10^5 Pa, 298.15 K) = 30.13 kJ/mol. Thus the reaction should not be favoured towards goethite formation. However, taking the global reaction pathway (1) + (2) gives a $\Delta_R G^\circ$ (10^5 Pa, 298.15 K) = −13.45 kJ/mol. Therefore, the complete reaction is in fact (Fig. 16A):

$$Fe^0 + 2H_2O = \alpha\text{-}FeOOH + \tfrac{3}{2}H_2 \quad (3)$$

In this case, siderite is only a transient product. Due to its very low solubility ($K_S = 2.1 \times 10^{-11}$), it precipitates very rapidly, before Fe^{2+} oxidation. The unfavoured reaction of Fe^{2+} oxidation into Fe^{3+} by H^+ or water is possible through catalysis by UV radiation (Burns, 1993). But our experiments have been conducted in a near complete darkness. Therefore, other mechanisms may be involved in the transformation. The constants of reactions (1) and (2) are, respectively:

$$K_1 = \frac{f_{H_2}}{f_{CO_2}} \quad (4)$$

$$\text{and } K_2 = f_{CO_2} \cdot \sqrt{f_{H_2}} \quad (5)$$

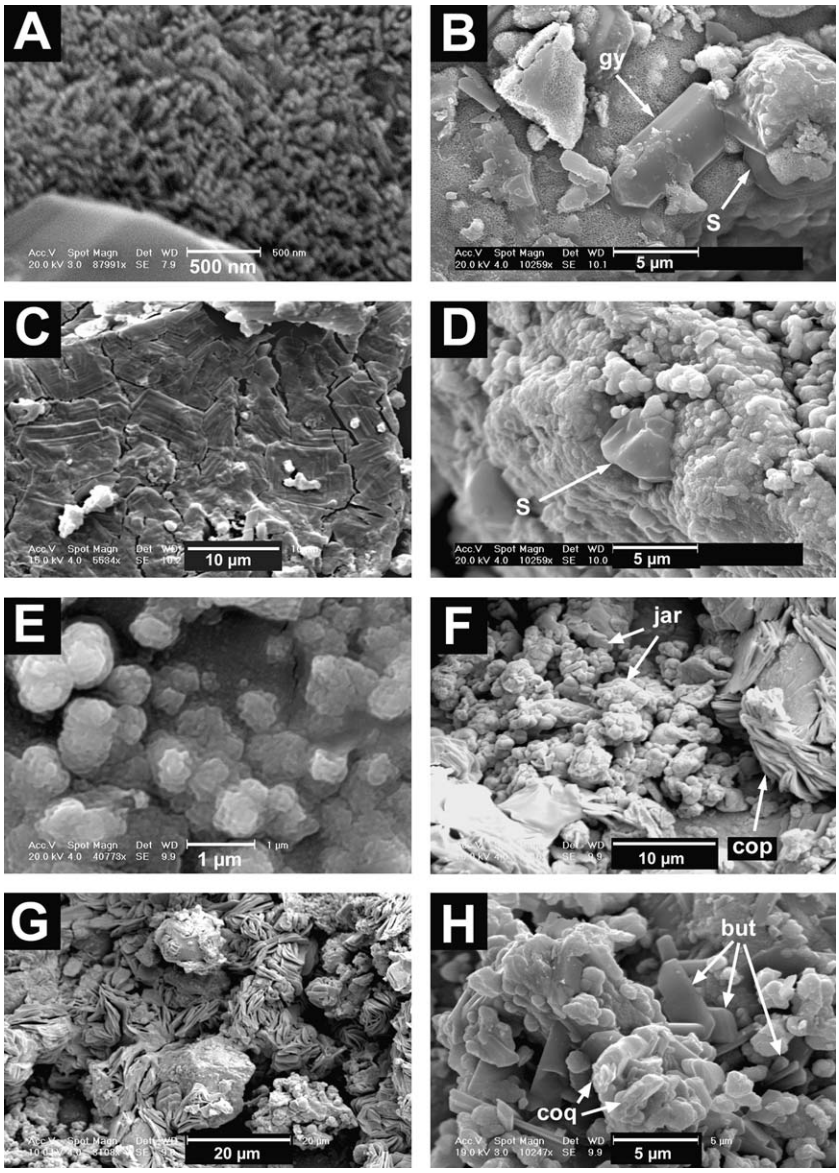

Fig. 8. SEM pictures of neoformed products on pyrrhotite. (A) goethite crystallites (HPo after 173 days in water atmosphere). (B) gypsum crystal (gy) close to a rounded crystal of elemental sulfur (S) (HPo after 173 days in water atmosphere). (C) Crystalline aggregate of melanterite (MPo after 259 days in water atmosphere). (D) Crystal of elemental sulfur (S) embedded in crusts of goethite (HPo after 173 days in peroxide atmosphere). (E) Close view of goethite crusts (HPo after 173 days in peroxide atmosphere). (F) Globular jarosite (jar) associated to aggregates of tabular copiapite (cop) crystals (MPo after 259 days in peroxide atmosphere). (G) Aggregates of tabular copiapite crystals (MPo after 259 days in peroxide atmosphere). (H) Accessory sulfates: thin tabular elongated crystals of butlerite/parabutlerite (but) associated to coarse thick tabular crystals of coquimbite (coq) (MPo after 259 days in peroxide atmosphere).

where f is the fugacity of gaseous CO_2 and H_2. Both equilibria depend on hydrogen fugacity. However, hydrogen is not confined in our experiments, and easily diffuses across the dessicator's wall, so that these heterogeneous reactions are not at equilibrium. Moreover, siderite formation is dependent on the first power of the hydrogen activity, but to its square root in the case of its transformation into goethite. Thus loss of hydrogen shifts the reactions towards the right hand side, but not at the same rate. This difference in the sensitivity of the chemical reactions to hydrogen fugacity results in the differential stabilization of siderite. Eq. (2) does not adequately explain the conversion of siderite into goethite. Indeed the actual mechanism may rather induce dissolution of siderite, indicated by etch pits on SEM pictures, aqueous oxidation of Fe^{2+} into ferrihydrite, evidenced by TEM and X-ray diffraction and then conversion of ferrihydrite into goethite.

4.2. Pyrrhotites

4.2.1. Water atmosphere

The initial reaction of pyrrhotite oxidation in acidic and moderately oxidizing conditions is the dissolution reaction (Fig. 16B):

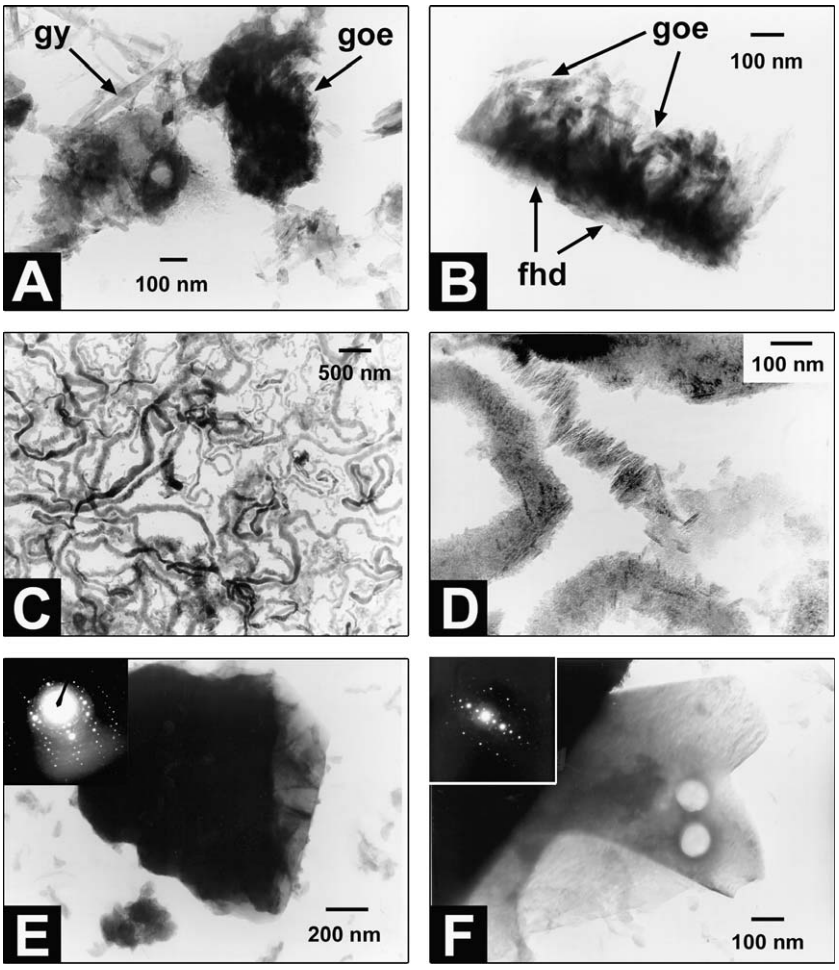

Fig. 9. TEM pictures of neoformed products on HPo. (A) small crystals of gypsum (gy) close to a cluster of goethite (goe) crystals (259 days in water atmosphere). (B) Close view of goethite (goe) crystals associated to its amorphous precursor, probably ferrihydrite (fhd) (259 days in water atmosphere). (C) Numerous filaments of elemental sulfur (259 days in peroxide atmosphere). (D) Close view of sulfur filaments evidencing the structure composed of parallel crystals (259 days in water atmosphere). (E) Jarosite crystal with diffraction pattern in the upper left corner (259 days in peroxide atmosphere). (F) Ferric sulfate, most probably coquimbite, with diffraction pattern in the upper left corner (259 days in peroxide atmosphere).

$$Fe_{1-x}S + 2H^+ = (1-x)Fe^{2+}{}_{(aq)} + H_2S_{(aq)} \quad (6)$$

However, the main sulfur species detected in the water atmosphere is elemental sulfur, implying an oxidation mechanism to further transform S^{2-} into S^0. The reaction (6) does not take into account the non-stoichiometry of pyrrhotite which contains small amounts of Fe^{3+}. Therefore, the reaction (6) can be rewritten as:

$$Fe_{1-x}S + 2H^+ = \frac{2x}{1-x}Fe^{3+}{}_{(aq)} + \frac{1-3x}{1-x}Fe^{2+}{}_{(aq)} + H_2S_{(aq)} \quad (7)$$

This reaction releases small amounts of Fe^{3+} into solution, which oxidizes H_2S to form elemental sulfur:

$$H_2S_{(aq)} + 2Fe^{3+}{}_{(aq)} = S^0{}_{(s)} + 2Fe^{2+}{}_{(aq)} + 2H^+ \quad (8)$$

Alternatively evolution of the system toward more oxidizing conditions due to the escape of H_2 may also induce oxidation of S^{2-} (in H_2S) into S^0. Moreover, Fe^{3+} is a better oxidant of pyrrhotite than H^+ or even O_2 (Moses et al., 1987; Janzen et al., 2000):

$$Fe_{1-x}S + 2Fe^{3+}{}_{(aq)} = (3-x)Fe^{2+}{}_{(aq)} + S^0{}_{(s)} \quad (9)$$

Both reactions (8) and (9) could explain the formation of elemental sulfur, observed in both pyrrhotites (Filippou et al., 1997; Pratt and Nesbitt, 1997; Janzen et al., 2000). All the previous reactions leave in solution substantial amounts of Fe^{2+}, which is in turn oxidized to form ferric (oxy)hydroxides, explaining the association between goethite and elemental sulfur. However, the weathering mechanism of pyrrhotite may be still more complex. Our study shows that metastable monoclinic pyrrhotite forms in the hexagonal pyrrhotite. This monoclinic phase accounts for the presence of sulfur-rich phases at the interface between fresh pyrrhotite and neoformed products (Mycroft et al., 1995; Mikhlin et al., 2002). The monoclinic phase is formed by the reaction:

$$Fe_{1-x}S + 2(0.125-x)Fe^{3+} = Fe_{0.875}S + 3(0.125-x)Fe^{2+} \quad (10)$$

Goethite is the main secondary iron (oxy)hydroxide, associated with lepidocrocite only in control samples. Lepidocrocite has been previously observed during aqueous

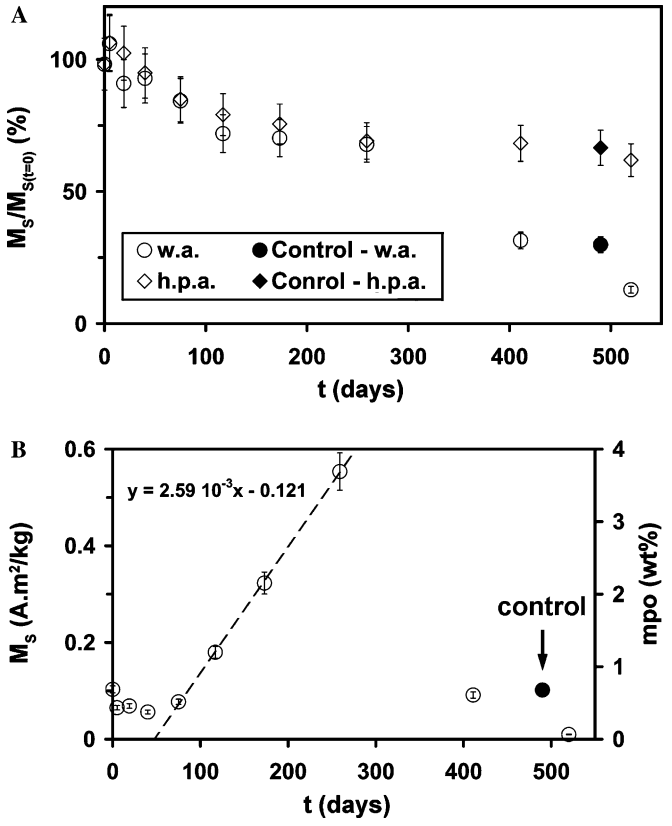

Fig. 10. Evolution of saturation magnetization M_S of pyrrhotites. (A) MPo in both atmospheres (w.a., water atmosphere; h.p.a., hydrogen peroxide atmosphere). (B) HPo in water atmosphere. On the right axis are represented the corresponding wt% contents in ferrimagnetic monoclinic pyrrhotite (mpo).

oxidation of pyrite controlled by carbonate ions (Nicholson et al., 1990; Descostes et al., 2002) and pyrrhotite in acidic water (Pratt and Nesbitt, 1997). However, the reason for its presence only in the control experiments remains unclear. Lepidocrocite forms by oxidation of dissolved Fe^{2+} by free O_2 at moderate pH between 5 and 7 (Schwertmann, 1985; Legrand et al., 2004), generally through a green rust (GR) precursor which is a Fe^{2+} and Fe^{3+} hydroxide containing anions like Cl^- or CO_3^{2-} (Cudennec and Lecerf, 2003; Legrand et al., 2004). The exposure of powders to atmospheric oxygen during periodic sampling, even for short periods of time, may have inhibited the formation of the GR precursor and then of lepidocrocite. Lepidocrocite can form at relatively low pH, even in the presence of dissolved CO_2, which generally promotes crystallization of goethite (Schwertmann, 1985). We suggest the formation of lepidocrocite through oxidation of a sulfate GR(SO_4^{2-}) due to the abundance of sulfur in the system:

$$4Fe^{2+} + 2Fe^{3+} + SO_4^{2-} + 12H_2O = {Fe^{2+}}_4{Fe^{3+}}_2(OH)_{12}SO_4 + 12H^+ \quad (11)$$

In Eq. (11), ${Fe^{2+}}_4{Fe^{3+}}_2(OH)_{12}SO_4$ corresponds to the GR(SO_4^{2-}) precursor (Refait et al., 2003; Bourrié et al., 2004). The transformation of GR(SO_4^{2-}) into ferric (oxy)hydroxides occurs through:

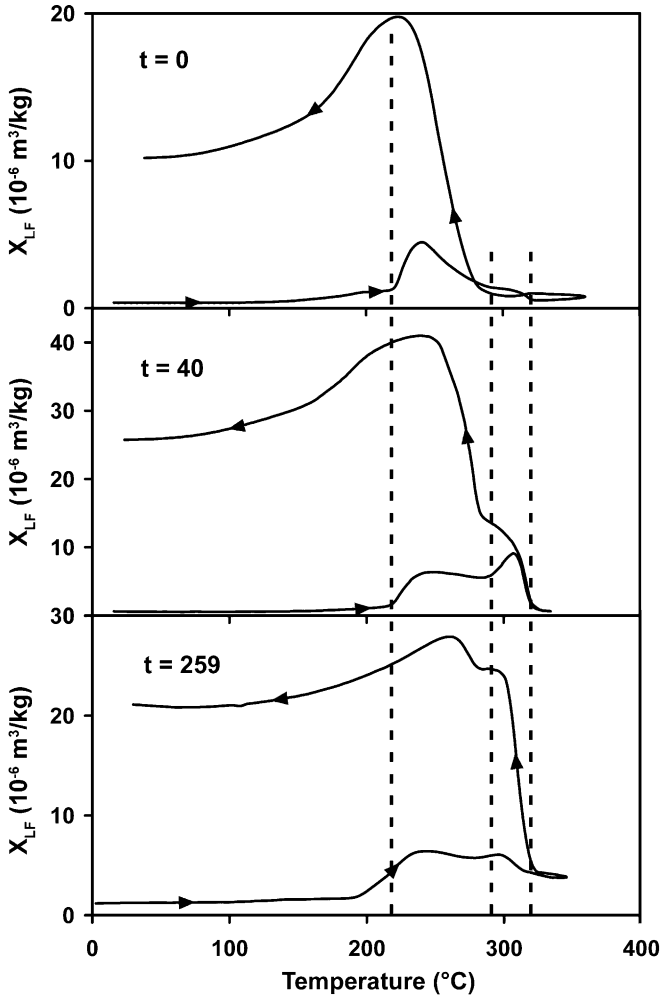

Fig. 11. χ_{LF} versus temperature curves of HPo weathered in water atmosphere, at $t = 0$, 40, and 259 days from top to bottom. The dashed lines give the three magnetic transitions relative to pyrrhotite, i.e., the γ-transition of the hexagonal pyrrhotite at 220 °C, the Curie temperature of the hexagonal pyrrhotite at 295 °C and the Curie temperature of the monoclinic pyrrhotite at 320 °C.

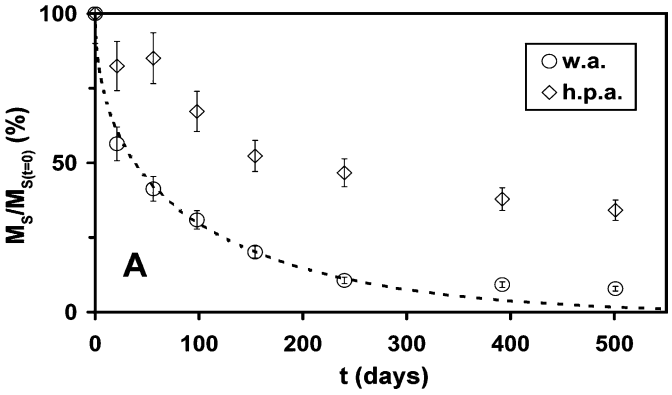

Fig. 12. Evolution of the M_S of the mixture (α-Fe + MPo) with weathering time in both atmospheres (w.a., water atmosphere; h.p.a., hydrogen peroxide atmosphere). The fit on M_S corresponds to application of the shrinking core model (SCM) as described in Section 4.3.

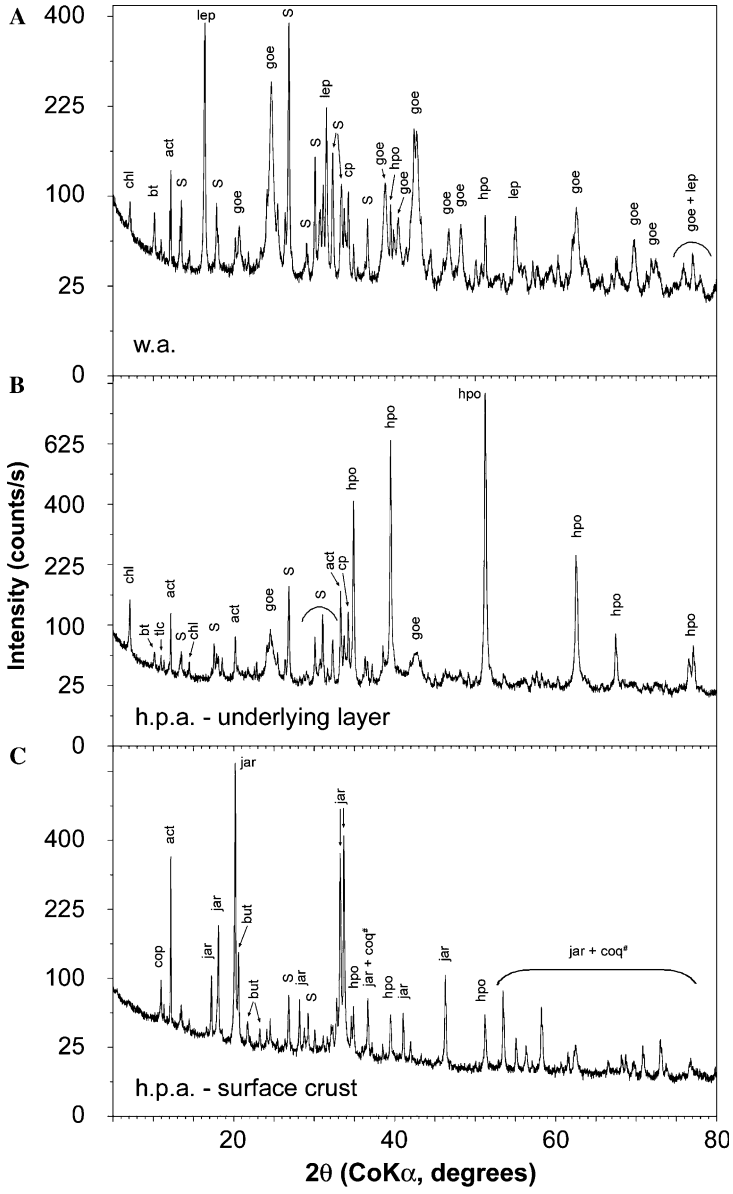

Fig. 13. X-ray diffraction patterns of HPo control sample (w.a., water atmosphere; h.p.a., hydrogen peroxide atmosphere). (A) w.a., (B) underlying layer in (h.p.a.), (C) surface crust in h.p.a. *Abbreviations:* act, actinolite; bt, biotite; but, butlerite/parabutlerite; chl, chlorite; cop, copiapite; coq, coquimbite; cp, chalcopyrite; goe, goethite; hpo, hexagonal pyrrhotite; jar, jarosite; lep, lepidocrocite; S, elemental sulfur; tlc, talc. #Most of the apparent peaks are in fact composite peaks of jarosite + coquimbite, especially at high values of 2θ.

$$Fe^{2+}{}_4Fe^{3+}{}_2(OH)_{12}SO_4 = 6FeOOH + SO_4{}^{2-} + 2H^+ + 2H_2 \quad (12)$$

In Eq. (12), FeOOH refers to goethite and lepidocrocite, both phases usually forming congruently in the reaction pathways.

Even if sulfur accumulates, representing 80–86% of the oxidized pyrrhotite, according to Janzen et al. (2000), a small fraction of S^0 is oxidized by Fe^{3+} into $S^{6+}$to form sulfates and GR($SO_4{}^{2-}$) formation:

$$S^0{}_{(s)} + 4H_2O + 6Fe^{3+}{}_{(aq)} = SO_4{}^{2-}{}_{(aq)} + 6Fe^{2+}{}_{(aq)} + 8H^+ \quad (13)$$

This small fraction of oxidized sulfur is a strong argument for the moderately oxidizing conditions in the water atmosphere. Due to the low water content, the saturation of Fe^{2+} sulfates is easily reached, and thus melanterite $FeSO_4{\cdot}7H_2O$ precipitates (Jerz and Rimstidt, 2004). XRD indicates a larger amount of melanterite formed on monoclinic pyrrhotite compared to the hexagonal phase (especially when comparing relative intensities of melanterite with other neoformed phases). This result is attributed to the higher Fe^{3+} content of monoclinic pyrrhotite, inducing larger release of Fe^{3+} which in turn can oxidize the elemental sulfur.

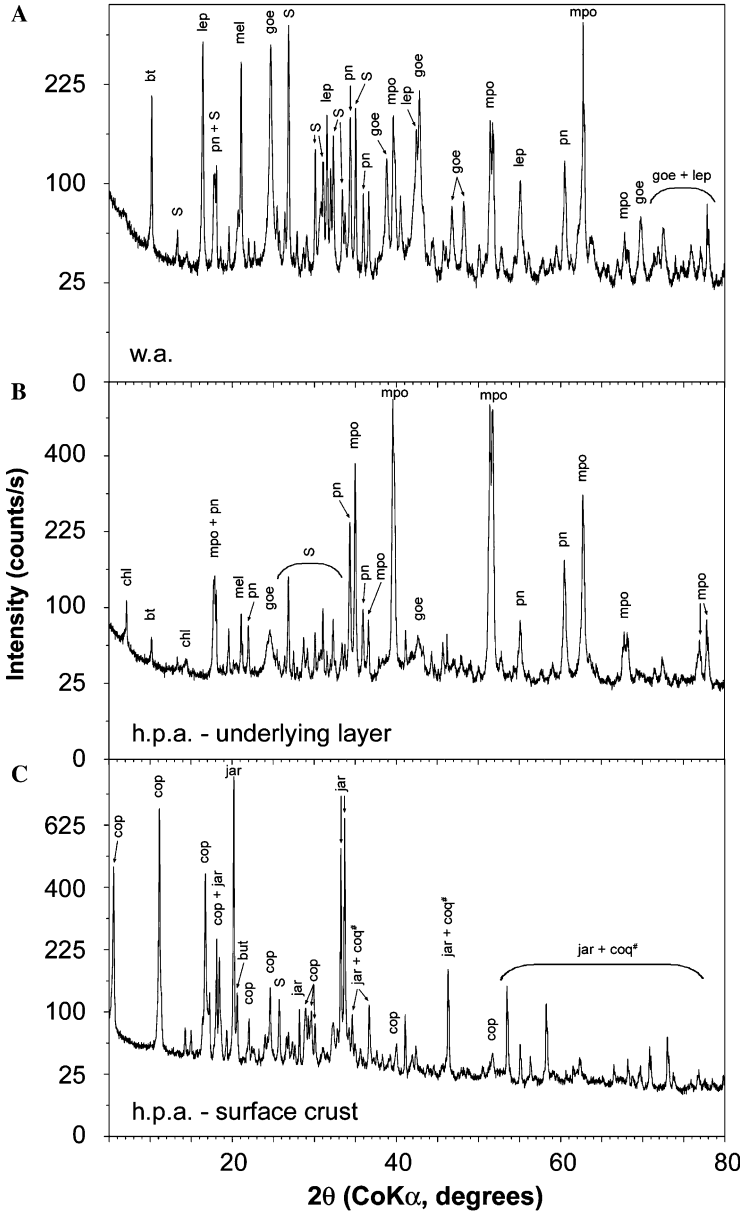

Fig. 14. X-ray diffraction patterns of MPo control sample (w.a., water; atmosphere, h.p.a., hydrogen peroxide atmosphere), (A) w.a., (B) underlying layer in (h.p.a.); (C) surface crust in h.p.a. *Abbreviations:* bt, biotite; but, butlerite/parabutlerite; chl, chlorite; cop, copiapite; coq, coquimbite; goe, goethite; jar, jarosite; lep, lepidocrocite; mel, melanterite; mpo, monoclinic pyrrhotite; pn, pentlandite; S, elemental sulfur. #Most of the apparent peaks are in fact composite peaks of jarosite + coquimbite, especially at high values of 2θ.

4.2.2. Hydrogen peroxide atmosphere

The mechanism of weathering in the peroxide atmosphere is driven by hydrogen peroxide H_2O_2 which is a strong oxidant, able to oxidize all the other phases present in the system (Fig. 16C). The first step of weathering is direct oxidation of pyrrhotite:

$$Fe_{1-x}S + H_2O_2 + 2H^+ = 1 - xFe^{2+}{}_{(aq)} + S^0{}_{(s)} + 2H_2O \quad (14)$$

Then both Fe^{2+} and S^0 are oxidized to Fe^{3+} and $SO_4{}^{2-}$:

$$2Fe^{2+}{}_{(aq)} + H_2O_{2(aq)} + 2H^+ = 2Fe^{3+}{}_{(aq)} + 2H_2O \quad (15)$$

$$S^0{}_{(s)} + 3H_2O_{2(aq)} = SO_4{}^{2-}{}_{(aq)} + 2H^+ + 2H_2O \quad (16)$$

Both $SO_4{}^{2-}$ and Fe^{3+} combine to form insoluble Fe^{3+}-sulfates: jarosite, copiapite and coquimbite:

$$3Fe^{3+} + 2SO_4{}^{2-} + 6H_2O = (H_3O)Fe_3(SO_4)_2(OH)_6 + 5H^+ \quad (17)$$

Eq. (17) is given for hydronium-jarosite formation, which is the main observed ferric sulfate, but copiapite, coquimbite and bulterite may form via a similar pathway. Jarosite and gypsum results from alteration of silicate traces present in natural HPo and MPo, and further remobilization of K^+ and Ca^{2+}ions. Biotite provides the main source of K^+, but is not sufficiently abundant to explain the abundance of jarosite in control samples (jarosite is very abundant in

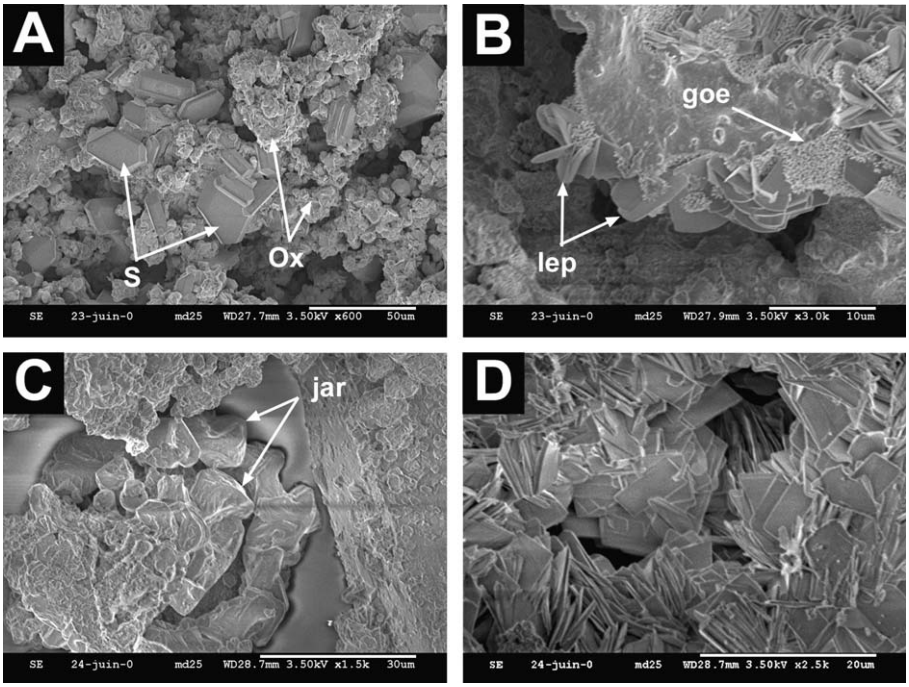

Fig. 15. SEM pictures of neoformed products on pyrrhotite control samples (w.a., water atmosphere; h.p.a., hydrogen peroxide atmosphere), (A) crystals of elemental sulfur (S) imbedded in iron (oxy)hydroxides (Ox); HPo in w.a. (B) Close view on iron (oxy)hydroxides showing relatively large platy crystals of lepidocrocite (lep) associated to nanocrystals of goethite (goe); MPo in w.a. (C) Crystalline aggregate of jarosite (jar); HPo in h.p.a. (D) Crystalline aggregate of copiapite tabular crystals; MPo in h.p.a.

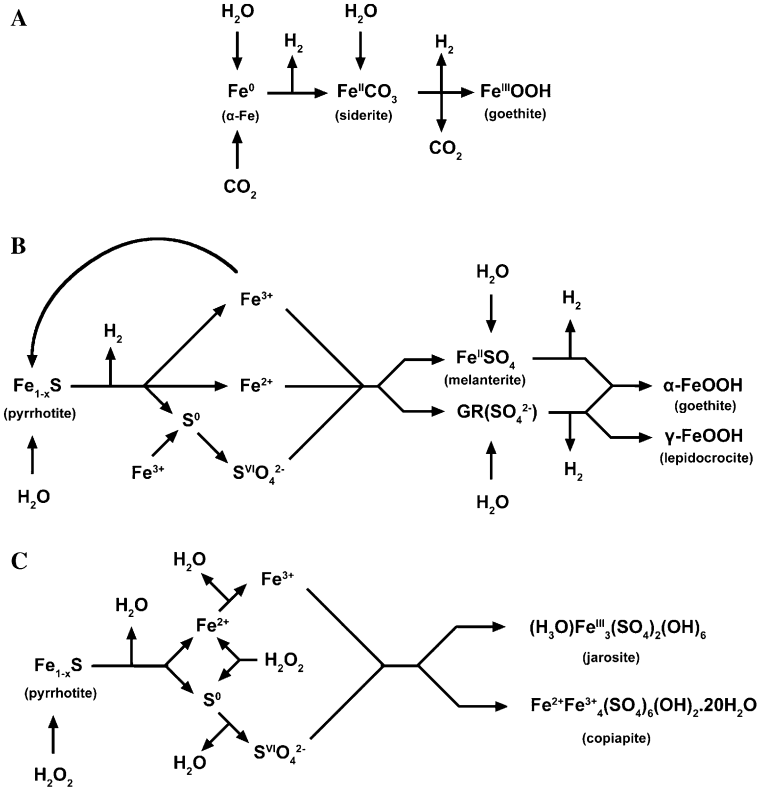

Fig. 16. Schematic summary of weathering reactions involved in our experiments. To improve clarity, only the main phases and chemical species have been represented. (A) Elemental iron α-Fe in water atmosphere, (B) pyrrhotite in water atmosphere. GR designs green rust, (C) pyrrhotite in hydrogen peroxide atmosphere.

the control samples, according to XRD). Therefore, jarosite is probably hydronium-jarosite, H_3O^+ being more abundant in the experiments.

Larger elemental sulfur abundance is observed in the water atmosphere, whereas it is only a trace phase in the peroxide atmosphere, because it is more readily oxidized by H_2O_2. Generally, the sulfate parageneses are different between the water atmosphere, dominated mainly by Fe^{2+}-sulfates (melanterite and/or rozenite) and the peroxide atmosphere dominated by Fe^{3+}-sulfates (jarosite, copiapite). The mineralogy of the "fresh" layer in pyrrhotite control samples weathered in the peroxide atmosphere is relatively similar to the mineralogy of samples weathered in water atmosphere. Only the surface of the powders undergoes strong oxidation of iron and sulfur in the peroxide atmosphere. The reaction assemblage in the peroxide atmosphere evolves from early metastable assemblages adjacent to the pyrrhotite to the more oxidized products forming the surface crust.

4.3. Weathering kinetics: the shrinking core model SCM

In the previous paper on the experimental weathering of α-Fe (Chevrier et al., 2004), we fitted the transformed iron mass with a $t^{-\frac{1}{2}}$ law, similar to Fick's law for diffusion. Indeed the main mechanism controlling the weathering of α-Fe seems to be the diffusion of the reactant through neoformed product layers (siderite and goethite). We try now to precisely define the kinetics mechanism using a more complete model, called the SCM or Shrinking Core Model (Wen, 1968). This model has been developed for heterogeneous reactions on spherical particles subjected to chemical alteration. This model has already been applied to pyrite and pyrrhotite alteration in aqueous media or weathering by moist air (Nicholson et al., 1990; Filippou et al., 1997; Jerz and Rimstidt, 2004). The SCM model includes three successive kinetic barriers (Wen, 1968): (1) the diffusion of the reactant to the surface across the film formed at the interface between the particle and the bulk fluid, (2) the chemical reaction at the interface leading to the neoformed product layer and (3) the diffusion of reactant across the porous neoformed product layer to reach the unreacted core. The complete equation is:

$$t = \frac{aRC_{S_0}}{C_{A_0}}\left[\frac{1}{3}\left(\frac{1}{k_{m_A}} - \frac{R}{D_{e_A}}\right)\left(1 - \frac{r_c^3}{R^3}\right) + \frac{R}{2D_{e_A}}\left(1 - \frac{r_c^2}{R^2}\right) + \frac{1}{ak_S C_{S_0}}\left(1 - \frac{r_c}{R}\right)\right] \quad (18)$$

With t: time, r_c: radius of the particle, R: radius of the particle at $t = 0$, C_{S_0}: mole fraction of solid reactant in the solid unreacted core, C_{A_0}: concentration of the reactant in the bulk fluid, a: stoichiometric coefficient representing the number of moles of fluid reactant reacting with 1 mole of solid reactant, k_{m_A}: mass transfer coefficient of the fluid reactant from the bulk fluid to the solid surface across the fluid film, k_S: chemical reaction constant and D_{e_A}: diffusion coefficient of reactant across the neoformed product layer. SEM observations of neoformed products show that they are systematically polycrystalline, with a small grain size (under $\leqslant 1$ μm for siderite and $\leqslant 0.5$ μm for goethite, cf. Fig. 3A). Therefore the diffusion is grain boundary diffusion rather than volume diffusion as would be the case if the neoformed layer was monocrystalline.

Eq. (18) can be transformed using the mass conversion rate through the relation:

$$Y = \frac{m}{m_0} = \frac{\rho\frac{4}{3}\pi r_c^3}{\rho\frac{4}{3}\pi R^3} \quad (19)$$

With ρ: density of the unreacted core and m/m_0: normalized mass of unreacted core. Moreover, Eq. (18) can be divided into three successive equations corresponding to the successive kinetic barriers:

(1) Control by fluid film:

$$t = \frac{aRC_{S_0}}{3k_{m_A}C_{A_0}}(1 - Y) \quad (20)$$

(2) Control by chemical reaction:

$$t = \frac{R}{k_S C_{A_0}}\left(1 - Y^{\frac{1}{3}}\right) \quad (21)$$

(3) Control by diffusion through the neoformed product layer:

$$t = \frac{aR^2 C_{S_0}}{6D_{e_A}C_{A_0}}\left(1 - 3Y^{\frac{2}{3}} + 2Y\right) \quad (22)$$

According to Wen (1968), defining the diffusion coefficient D_{e_A} on the surface area of the unreacted core allows the Eq. (22) to be rearranged as:

$$t = \frac{aR^2 C_{S_0}}{2D_{e_A}C_{A_0}}\left(1 - Y^{\frac{1}{3}}\right)^2 \quad (23)$$

We consider the diffusion through the fluid film to be instantaneous, as the water is supposed to be equilibrated with the atmosphere. So we limit the model to the chemical reaction and the diffusion through the neoformed products layer. The data can be linearized by representing the data in a log–log plot:

$$\ln(t) = f\left[\ln\left(1 - Y^{\frac{1}{3}}\right)\right] \quad (24)$$

All analytical methods employed in this study show that α-Fe weathering stops after 259 days, and the α-Fe + MPo mixture after 240 days. Therefore, we apply the SCM model until these points, i.e. on the period during which there is a reaction. Blocking of the reactions is discussed in the Section 4.4. Application of the Eq. (24) to α-Fe from 40 to 259 days shows a slope of 1.34 suggesting a combination between chemical reaction and diffusion processes (Fig. 17A). In fact, the data on Fig. 17A could be interpreted as

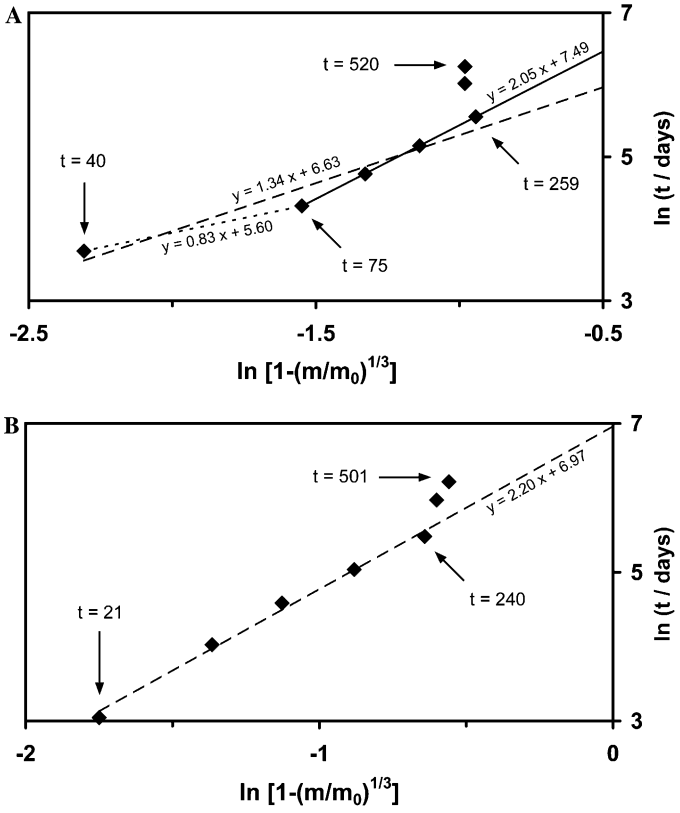

Fig. 17. Plot of $\ln[1-(m/m_0)^{1/3}]$ versus $\ln(t)$, with m/m_0 being the rate of initial mass transformed into neoformed products and t the time in days. (A) α-Fe (dashed line, regression from 40 to 259 days; dotted line, from 40 to 75 days and full line, from 75 to 259 days). (B) Mixture of α-Fe and MPo.

indicating two successive mechanisms. From 40 to 75 d the slope is 0.83, close to 1, probably due to control of the chemical reaction by siderite formation, although we admit that the presence of only two data points in this region makes this assumption speculative. From 40 to 259 d, the slope of the graph is 2, implying control by the diffusion through the siderite layer. Application of the SCM model to a mixture of α-Fe + MPo from 0 to 240 d yields a slope of 2.20 (Fig. 17B), indicating that the kinetics are also controlled by the diffusion through neoformed layers. This corresponds only to α-Fe weathering as it accounts for 95% of the M_S which is used to determine the m/m_0 ratio. The resulting curves are presented in Fig. 1 for α-Fe and in Fig. 12 for the mixture (α-Fe + MPo). According to Eq. (1), the mechanism corresponds to diffusion through the siderite layer of H^+, which are the electron acceptors responsible for the oxidation of Fe^0 to Fe^{2+}. This is probably also the case for the mixture, even if the composition of the neoformed layer may be more complex due to the presence of sulfates.

Using the curves extrapolated from the fit by the SCM model, it is possible to determine the time for complete conversion t_f, defined by $r_c = 0$ (or $Y = 0$). The t_f determined are 43,000 h and 22,000 h for α-Fe and (α-Fe + MPo), respectively. Thus the diffusion coefficient D_{e_A} of H^+ in the siderite layer can be calculated using the following equation for diffusion control:

$$t_f = \frac{aR^2 C_{S_0}}{2D_{e_A} C_{A_0}} \tag{25}$$

We use the following values: $a = 2$ as 2 mole of H^+ ions react with 1 mole of α-Fe to form Fe^{2+} and then $FeCO_3$; $C_{S_0} = 1$ for α-Fe as the unreacted core is composed of 100% Fe, but we use $C_{S_0} = 0.5$ to model the mixture of 50 wt% α-Fe and 50 wt% of MPo; $C_{A_0} = [H^+] = 1.197 \times 10^{-4}$ mol/L, which is equivalent to 2.154×10^{-6} mole of H^+ per mole of water; R = 5μm, which is the grain size given by the manufacturer. Then we obtain for α-Fe $D_{e_A} = 2.71 \times 10^{-10}(\pm 40\%)\mathrm{m}^2/\mathrm{h}$ and for the mixture $D_{e_A} = 2.69 \times 10^{-10}(\pm 63\%)\mathrm{m}^2/\mathrm{h}$. The similarity of these values indicates that diffusion of H^+ through the siderite layer is controlling the mechanism of weathering in both the cases of α-Fe and the mixture (α-Fe + MPo). The presence of other alteration products does not appear to influence the diffusion rate, which also favours grain boundary diffusion. To our knowledge, the SCM model has not been applied to the alteration of elemental iron. Nevertheless, a diffusion coefficient has been determined for O^{2-} diffusion through a 0.6 μm thick oxide layer formed on pyrite composed of lepidocrocite and maghemite, leading to $D_{e_A} = 1.08 \times 10^{-12}(\pm 28\%)\mathrm{m}^2/\mathrm{h}$ (Nicholson et al., 1990). Nicholson et al. (1990) assumed their relatively high value was due to diffusion through a polycrystalline, non-compact layer, but not through a porous "clay-like" layer for which diffusion coefficients would have been 3 to 4 times higher. The value obtained in this study is about 50 times higher than the Nicholson et al. value, a result that is attributable to the smaller size of the H^+ ion which enables it to diffuse more rapidly through the neoformed product layer.

4.4. Model uncertainties

The SCM model, as described by (Wen, 1968), is based on reaction kinetics of the first order. However data for α-Fe weathering in the range 19–75 d are much better fitted by a second order reaction kinetics curve (Fig. 1):

$$Y = \frac{m}{m_0} = \frac{1}{1 + m_0 k_S (t - t_0)} \tag{26}$$

with $t_0 = 19$ days, corresponding to the beginning of the chemical reaction. From the data on the Fe^0 consumption, and Eq. (26), determination of k_S yields 7.75×10^{-5} (±29%) $\mathrm{g}^{-1}/\mathrm{h}$. The second order of reaction determined from the data corresponds to the stoichiometric coefficient of H^+ in the equation:

$$Fe^0 + 2H^+ \xrightarrow{k_1} Fe^{2+} + 2H_2 \tag{27}$$

this indicates that the reaction of α-Fe and H^+ is an elementary reaction and the kinetic equation can be rewritten as:

$$\frac{d[H^+]}{dt} = -k_1[H^+]^2 \quad (28)$$

where $[H^+]$ is the concentration of protons at the surface of the α-Fe particles and k_1 is the reaction constant. In molar equivalent $k_S = k_1 = 1.38 \times 10^{-6}$ mol^{-1}/h. We do not consider the reverse reaction as the H_2 produced is lost from the system, shifting the reaction towards the production of Fe^{2+}.

The initial period of α-Fe weathering, from 0 to 19 d, is not described by the SCM model. This period, during which no transformation is detectable, may correspond to an "activation" period, necessary for the formation of fluid films and initiation of weathering. The mixture of α-Fe + MPo does not show any activation period, neither a chemical control of the weathering mechanism (period from 19 to 75 d for α-Fe). Rapid release of oxidant ions by pyrrhotite weathering (Fe^{3+}) may have improved α-Fe weathering.

We could not apply the SCM model to pyrrhotite weathering, because of the large range in grain size which results from the preparation method (i.e. manual grinding). This situation requires application of the model with a statistical distribution of grain size, and is much more difficult to calculate. Nevertheless, the observation of coatings on grains by SEM, and the M_S profile of MPo suggest a diffusion-controlled mechanism.

Weathering initiates at reactive sites with the highest surface energy, such as grain edges, corners, pits, cleavages and fractures (McKibben and Barnes, 1986). Surface defects increase specific surface areas, enhancing weathering (Janzen et al., 2000). SEM observations show that sulphide grains are highly fractured with complex morphologies whereas α-Fe particles are spherical with a very uniform surface. Such quasi-perfectly shaped particles have very low concentrations of surface defects where weathering can initiate. Janzen et al. (2000) found that the specific surface area of pyrrhotite is 6–40 times greater than the theoretical geometric specific area calculated for spherical particles (i.e. similar to the α-Fe particles). Then the surface state may explain why α-Fe remains unweathered in the peroxide atmosphere, and takes as long as 20 days to begin to alter in the water atmosphere, whereas pyrrhotite powders are more readily weathered.

H_2O_2 is a stronger oxidant than water so that the rate of oxidation of the grains should be increased compared to oxidation driven only by water. In our experiments rapid oxidation of pyrrhotite by hydrogen peroxide is indicated by crust formation after only 5 d. However, the high oxidant property of H_2O_2 is not sufficient to explain our observations. M_S data indicates that 70 wt% MPo is transformed after 411 d in the water atmosphere, against 30 wt% MPo after 411 d in the peroxide atmosphere. Furthermore, α-Fe remains unaltered in the peroxide atmosphere. This result can be partly explained by the preferential catalytic deoxygenation of H_2O_2 by α-Fe and sulfides, rather than their oxidation. Studies on pyrite oxidation rates show that H_2O_2 decomposition occurs at a similar rate (McKibben and Barnes, 1986). Such reactions could have limited the oxidation effect of H_2O_2.

There are also some discrepancies between the SCM model and our data on α-Fe and mixture at the end of the experiments. Indeed the remaining mass after 259 d for α-Fe and after 240 d for (α-Fe + MPo) is constant and higher than the values predicted by the SCM model (Figs. 1 and 12). In both cases, the inhibition of the reaction occurs when siderite has been completely converted into goethite. A first explanation to this result is that the diffusion coefficient of H^+ in the goethite layer is much lower than in siderite. But this seems unlikely when considering that the diffusion is grain boundary controlled. Alternatively a more complex oxidation process for α-Fe may be responsible for such a passivation mechanism. Indeed if H^+ is the main component responsible for Fe^0 oxidation into Fe^{2+}, then of course CO_3^{2-} ions are also necessary for siderite precipitation. However, the SCM model does not take account a change in the diffusion coefficient, due to different products, nor does it account for the combined diffusion of several ions. Goethite could then be an impermeable product for CO_3^{2-} ions going to the core where Fe^{2+} ions are produced, or for Fe^{2+} to reach the surface of particles. If goethite acts as a barrier between Fe^{2+} and CO_3^{2-}, then the siderite formation is prevented and the reaction is inhibited, even if H^+ is the main reactant.

5. Implications for mars

5.1. Weathering model and evolution of martian surface conditions

As suggested by several studies, the presence of a primary martian atmosphere may have resulted from large amounts of gas released by volcanic activity (Pollack et al., 1987; Forget and Pierrehumbert, 1997; Phillips et al., 2001). This atmosphere was probably composed of CO_2, H_2O and SO_2 (Postawko and Kuhn, 1986). The resultant intense greenhouse effect may have stabilized liquid water on the surface of Mars, an hypothesis possibly confirmed by the recent observation of clays on the south noachian crust (Poulet et al., 2005). Such conditions are simulated by our experiments with high CO_2 and H_2O partial pressures (water atmosphere). Our results confirm previous thermodynamic models indicating that weathering under such reducing conditions results in large amounts of Fe^{2+} in solution, promoting the formation of Fe^{2+}-bearing minerals, like siderite (Catling, 1999) or ferrous (oxy)hydroxides like green rusts. Nevertheless, in our experiments goethite forms as the main iron (oxy)hydroxide, frequently associated to its precursor ferrihydrite, and sometimes to lepidocrocite. These phases are the main ferric end-products of all experimental weathering processes, confirming previous models of sulfides and iron metal weathering (Burns and Fisher, 1990; Burns, 1993; Abdelmoula et al., 1996). Evolution of the martian atmo-

sphere from reducing to more oxidizing conditions may have induced complete conversion of Fe^{2+} phases (green rusts and siderite) to lepidocrocite and goethite (Banin et al., 1993; Catling, 1999). Lepidocrocite formation seems particularly favoured on a basaltic substrate (Posey-Dowty et al., 1986), probably because of higher pH than for acidic igneous rocks. Thus goethite and lepidocrocite should dominate the weathering mineralogy of early Mars (Chevrier et al., 2004). Spectra of the martian surface suggest that both phases could be present (Kirkland and Herr, 2000; Morris et al., 2000) possibly as remnants of weathering on early Mars. However, the nature of the oxidant responsible for the evolution of the oxidation state of the surface is still unknown. Photodissociation of H_2O and further thermal escape of H_2 are efficient mechanisms to produce O_2 which equilibrates with the primary hydrosphere and oxidizes Fe^{2+} precursors into ferric (oxy)hydroxides (Catling and Moore, 2003; Lammer et al., 2003). However, some calculations have shown that O_2 would have always remained a trace component of the martian atmosphere (Catling and Moore, 2003). Our study shows that O_2 may not be required for the oxidation of Fe^{2+} into Fe^{3+}. Water and H^+ may have driven all oxidation reactions, promoted in an acidic media resulting from the dissolution of gas produced by volcanic activity (CO_2 and SO_2). These reactions are efficient in producing large amounts of H_2, which escapes from Mars, while oxygen, in the form of OH^- hydroxyl groups, remains trapped in oxidized phases. The progressive escape of H_2 from Mars may have forced the oxidation of the surface, in a similar way as this process may have been responsible for the irreversible oxidation of the primitive terrestrial atmosphere (Catling et al., 2001). Nevertheless, if possible this mechanism may have dominated until the strong oxidants became sufficient in abundance. The results with a peroxide atmosphere show that our mineralogical results are very similar to the recent observations of the Martian surface, and especially Meridiani Planum (iron (oxy)hydroxides, jarosite, gypsum). Therefore strong oxidants may have played a dominant role in the oxidation of these formations.

5.2. Evolution of iron (oxy)hydroxides on Mars

As no hematite is formed in our experiments, it may not have been formed by direct weathering on Mars, but it is rather a transformation product of ferric (oxy)hydroxides. Ferric (oxy)hydroxides such as goethite or lepidocrocite are thermodynamically unstable under current conditions on Mars, due to the very low activity of water and gas pressures (Gooding, 1978; Burns, 1993). Instead, the main stable ferric phase is hematite (Gooding, 1978). The direct transformation of goethite into hematite at martian surface temperatures, if thermodynamically favoured, is strongly kinetically inhibited (Schwertmann, 1985). However, the martian regolith may have aged under such conditions for much larger periods than any soil on the Earth, so the very slow transformation of goethite to hematite may still be possible. Alternatively, the direct transformation of goethite to hematite may be promoted by high temperature. A possible origin to the layers of "grey crystalline hematite" observed by TES onboard Mars Global Surveyor (Christensen et al., 2000; Hynek et al., 2002) and for Maridiani Planum "blueberries" is through burial and subsequent thermal recrystallization of basaltic rocks previously altered by water (Catling and Moore, 2003; Christensen and Ruff, 2004). Laboratory experiments show that the best precursor for the hematite spectra is goethite heated to about 300 °C (Glotch et al., 2004). Ferrihydrite is the first phase to form in weathering processes, whatever the climate, and is a precursor to goethite and hematite. Then its formation on Mars is strongly suggested (Banin et al., 1993; Bishop and Pieters, 1995; Banin, 1996) and seems to fit some reflectance measurements (Evans and Adams, 1980; McSween et al., 1999). Weathering in conditions of very low water activity may favour phases of low crystallinity such as ferrihydrite (Schwertmann et al., 1999). However, ferrihydrite is generally unstable in solution, and is subjected to further evolution into crystalline phases, depending on surface conditions: pH and surface temperature (Torrent et al., 1982; Schwertmann, 1985; Schwertmann et al., 1999). Hematite is favoured at relatively high temperatures and high pH, whereas goethite dominates at low pH and low temperature (Schwertmann et al., 1999). On Earth, such variations in local chemistries and climate explain changes in goethite/hematite ratios in lateritic profiles (Tardy and Nahon, 1985; Tardy et al., 1988; Fernandez-Remolar et al., 2004) as well as in alteration products of basalt under dry polar climates (Bender Koch et al., 1995).

5.3. Magnetic phases on mars

Our study provides strong arguments about the possible processes forming strongly magnetic phase(s). Magnetite appears to be very stable in these experimental conditions. As this phase has been observed in primary rocks on Mars (Morris et al., 2004; Goetz et al., 2005), its presence in the martian regolith may result from conservation through weathering processes. Another pathway to form strongly magnetic spinel is provided by the possible presence of lepidocrocite. Heating lepidocrocite induces the formation of maghemite, a pathway already invoked to account for the formation of maghemite on Mars (Morris et al., 1998). Therefore, some process of burial and thermal recrystallization that may have been responsible for the formation of hematite from goethite (Glotch et al., 2004), could also form hematite plus maghemite from lepidocrocite. Finally the presence of elemental iron resulting from meteoritic bombardment, especially from IDP's, and protected by secondary coatings, could also account for some magnetic particles. But the stability of iron will largely depend on its weathering kinetics, which can be however inhibited by secondary coatings, as in these experiments,

by temperature which slows down diffusion processes, or by the presence of nickel. Indeed Ni increases significantly the weathering resistance of Fe–Ni alloys in meteorites samples (Lee and Bland, 2004).

5.4. Sulfur and sulfates in the martian regolith

Sulfur is an abundant element in the martian regolith, with concentrations around 8% SO_3 (Foley et al., 2003; Gellert et al., 2004), due to the presence of sulfates. According to our experiments, sulfur assemblages are dominated by elemental sulfur and Fe^{2+}-sulfates in the weakly oxidizing water atmosphere whereas Fe^{3+}-sulfates (jarosite and copiapite) prevail in the strongly oxidizing peroxide atmosphere. Jarosite is an important phase of Meridiani Planum deposits (Klingelhöfer et al., 2004). Our results suggest that oxidative weathering of pyrrhotite/iron sulfides may have played an important role in the formation of sulfate enriched formations (Burns and Fisher, 1990). Other models explain the abundance of sulfates by volatile-rich hydrothermal fluid contamination, resulting from intense volcanism (Newsom and Hagerty, 1997; Newsom et al., 1999). However, unlike our model, these models fail to explain the abundance of ferric (oxy)hydroxides in the regolith.

6. Conclusions

This experimental study of weathering of iron-bearing primary phases provides new insight into possible processes occurring under early and present martian conditions:

(1) Magnetite is the only stable phase throughout the whole duration of the experiment, and may then be conserved during weathering processes. Other strongly magnetic phases that may be present in the martian regolith include traces of metastable exogenic iron, protected by varnishes of ferric (oxy)hydroxides. Metal may accumulate in the martian regolith, persisting metastably due to sluggish kinetics of transformation at low temperature.
(2) Goethite is the principal iron (oxy)hydroxide in all experiments, forming in slightly and strongly oxidizing atmospheres. Goethite is the end-product of various alteration pathways involving metastable phases. Under more reducing conditions, lepidocrocite may be associated with goethite. Both (oxy)hydroxides are therefore likely to have formed by weathering processes on early Mars. Further evolution of these precursors (dehydration, burial metamorphism) could explain various in situ observations of hematite and possibly maghemite on the martian surface.
(3) The correspondence between sulfates produced in our experiments (jarosite), and those observed in situ on Mars indicate that sulfides may have played a significant role in the formation of the sulfate deposits.
(4) Weathering on early Mars may have started in slightly oxidizing conditions, inducing formation of Fe^{2+}-bearing phases as sulfates (melanterite), siderite and green rusts, associated with elemental sulfur in the case of sulfur-rich primary bedrock. Further evolution towards more oxidizing surface conditions may have forced the evolution of these phases into oxidized equivalents, i.e., ferric (oxy)hydroxides and ferric sulfates. These transformations may have been promoted by strong oxidants such as hydrogen peroxide, which are continuously produced by photochemistry in the atmosphere.
(5) Free oxygen is not required for weathering on Mars. Water is able to oxidize primary phases, and explain the formation of secondary oxidized ferric species. Moreover, water-driven process provides an efficient mechanism for hydrogen production, which escapes from the planet's atmosphere. H_2 escape induces then irreversible oxidation of the surface of Mars.

Acknowledgments

We thank Jean-Pierre Lorand and the Museum National d'Histoire Naturelle de Paris for having provided the sample of MPo. We are also indebted to M. Legoff and P. Henry from St. Maur Observatory for their providing access to thermomagnetic curve measurements, as well as A. Tonetto and R. Notonier from Faculty of St. Charles, Marseille for their assistance in using the environmental SEM. Finally we want to thank Dr. R.A. Wogelius as well as both anonymous reviewers that helped by their suggestions to improve the quality of this manuscript. The planetology program from INSU/CNES supported this work.

Associate editor: Roy A. Wogelius

References

Abdelmoula, M., Refait, P., Drissi, S.H., Mihe, J.P., Génin, J.-M.R., 1996. Conversion electron Mössabuer spectroscopy and X-ray diffraction studies of the formation of carbonate-containing green rust one by corrosion of metallic iron in $NaHCO_3$ and ($NaHCO_3 + NaCl$) solutions. *Corros. Sci.* **38** (4), 623–633.

Allan, J.E.M., Coey, J.M.D., Resende, M., Fabris, J.D., 1988. Magnetic properties of iron-rich oxisols. *Phys. Chem. Miner.* **15**, 470–475.

Baldridge, A.M., Calvin, W.M., 2004. Hydratation state of the Martian coarse-grained hematite exposures: implications for their origin and evolution. *J. Geophys. Res.* **109** (E04S90).

Banin, A., 1996. The missing crystalline minerals in Mars soils. *Adv. Space Res.* **18** (12), 12233–12240.

Banin, A., Ben-Schlomo, T., Margulies, L., Blake, D.F., Mancinelli, L., Gehring, E.U., 1993. The nanophase iron mineral(s) in Mars soil. *J. Geophys. Res.* **98** (E11), 20831–20853.

Bender Koch, C., Morup, S., Madsen, M.B., Vistisen, L., 1995. Iron-containing products of basalt in a cold-dry climate. *Chem. Geol.* **122**, 109–119.

Bertelsen, P., Goetz, W., Madsen, M.B., Klinch, K.M., Hviid, S.F., Knudsen, J.M., Gunnlaugsson, H.P., Merrison, J., Nornberg, P., Squyres, S.W., Bell III, J.F., Herkenhoff, K.E., Gorevan, S.

Yen, A.S., Myrick, T., Klingelhöfer, G., Rieder, R., Gellert, R., 2004. Magnetic properties experiments on the Mars exploration rover spirit at Gusev Crater. *Science* **305** (5685), 827–829.

Bishop, J.L., Pieters, C.M., 1995. Low-temperature and low atmospheric pressure infrared reflectance spectroscopy of Mars soil analog materials. *J. Geophys. Res.* **100** (E3), 5369–5379.

Bland, P.A., Smith, T.B., 2000. Meteorite accumulation on Mars. *Icarus* **144**, 21–26.

Bourrié, G., Trolard, F., Refait, P., Feder, F., 2004. A solid-solution model for Fe(II)–Fe(III)–Mg(II) green rusts and fougerite and estimation of their gibbs free energies of formation. *Clays Clay Miner.* **52** (3), 382–394.

Burns, R.G., 1993. Rates and mechanisms of chemical weathering of ferromagnesian silicate minerals on Mars. *Geochim. Cosmochim. Acta* **57**, 4555–4574.

Burns, R.G., Fisher, D.S., 1990. Iron-sulfur mineralogy of Mars : magmatic evolution and chemical weathering products. *J. Geophys. Res.* **95** (B9), 14415–14421.

Burns, R.G., Fisher, D.S., 1993. Rates of oxidative weathering on the surface of Mars. *J. Geophys. Res.* **98** (E2), 3365–3372.

Carpenter, R.H., 1974. Pyrrhotite isograd in southeastern Tennessee and southwestern North Carolina. *Geol. Soc. Am. Bull.* **85**, 451–456.

Catling, D.C., 1999. A chemical model for evaporites on early Mars: possible sedimentary tracers of the early climate and implications for exploration. *J. Geophys. Res.* **104** (E7), 16453–16469.

Catling, D.C., Moore, J.M., 2003. The nature of coarse-grained crystalline hematite and its implications for the early environment of Mars. *Icarus* **165**, 277–300.

Catling, D.C., Zahnle, K.J., McKay, C.P., 2001. Biogenic methane, hydrogen escape, and the irreversible oxidation of early Earth. *Science* **293**, 839–843.

Chevrier, V., Rochette, P., Mathé, P.-E., Grauby, O., 2004. Weathering of iron rich phases in simulated Martian atmospheres. *Geology* **32** (12), 1033–1036.

Christensen, P.R., Bandfield, J.L., Bell III, J.F., Gorelick, N., Hamilton, V.E., Ivanov, A., Jakosky, B.M., Kieffer, H.H., Lane, M.D., Malin, M.C., McConnochie, T., McEwen, A.S., McSween Jr., H.Y., Mehall, G.L., Moersch, J.E., Nealson, K.H., Rice Jr., J.W., Richardson, M.I., Ruff, S.W., Smith, M.D., Titus, T.N., Wyatt, M.B., 2003. Morphology and composition of the surface of Mars : Mars Odyssey THEMIS results. *Science* **300**, 2056–2061.

Christensen, P.R., Banfield, J.L., Clark, R.N., Edgett, K.S., Hamilton, V.E., Hoefen, T., Kieffer, H.H., Kuzmin, R.O., Lane, M.D., Malin, M.C., Morris, R.V., Pearl, J.C., Pearson, R., Roush, T.L., Ruff, S.W., Smith, M.D., 2000. Detection of crystalline hematite mineralization on Mars by the thermal emission spectrometer: evidence for near-surface water. *J. Geophys. Res.* **105** (E4), 9623–9642.

Christensen, P.R., Morris, R.V., Lane, M.D., Bandfield, J.L., Malin, M.C., 2001. Global mapping of Martian hematite mineral deposits : remnants of water-driven processes on early-Mars. *J. Geophys. Res.* **106** (E10), 23873–23885.

Christensen, P.R., Ruff, S.W., 2004. Formation of the hematite-bearing units in Meridiani Planum: evidence for deposition in standing water. *J. Geophys. Res.* **109** (E08003).

Clancy, R.T., Sandor, B.J., Moriarty-Schieven, G.H., 2004. A measurement of the 362 GHz absorption line of Mars atmospheric H_2O_2. *Icarus* **168** (1), 116–121.

Cliff, G., Lorimer, G.W., 1975. The quantitative analysis of thin specimens. *J. Microsc.* **103**, 203–207.

Cudennec, Y., Lecerf, A., 2003. Etude des mécanismes de formation des oxy-hydroxydes de fer; hypothèses de transformations topotactiques. *C.R. Chimie* **6**, 437–444.

Dekkers, M.J., 1988. Some rockmagnetic parameters for natural goethite, pyrrhotite and fine-grained hematite. Ph.D. thesis, Utrecht University, The Netherlands.

Descostes, M., Beaucaire, C., Mercier, F., Savoye, S., Sow, J., Zuddas, P., 2002. Effect of carbonate ions on pyrite (FeS2) dissolution. *Bull. Soc. Geol. Fr.* **173** (3), 265–270.

Encrenaz, T., Bézard, B., Greathouse, T.K., Richter, M.J., Lacy, J.H., Atreya, S.K., Wong, A.S., Lebonnois, S., Lefèvre, F., Forget, F., 2004. Hydrogen peroxide on Mars: evidence for spatial and seasonal variations. *Icarus* **170**, 424–429.

Evans, D.L., Adams, J.B., 1980. Amorphous gels as possible analogs to Martian weathering products. *Proc. Lunar Planet. Sci.* **11**, 757–763.

Fernandez-Remolar, D., Gomez-Elvira, J., Gomez, F., Sebastian, E., Martiin, J., Manfredi, J.A., Torres, J., Gonzalez Kesler, C., Amils, R., 2004. The Tinto River, an extreme acidic environment under control of iron, as an analog of the Terra Meridiani hematite site of Mars. *Planet. Space Sci.* **52**, 239–248.

Filippou, D., Konduru, R., Demopoulos, G.P., 1997. A kinetic study on the acid pressure leaching of pyrrhotite. *Hydrometallurgy* **47**, 1–18.

Flynn, G.J., McKay, D.S., 1990. An assessment of the meteorite contribution to the Martian soil. *J. Geophys. Res.* **95**, 14497–14509.

Foley, C.N., Economou, T., Clayton, R.N., 2003. Final chemical results from the Mars Pathfinder alpha proton X-ray spectrometer. *J. Geophys. Res.* **108** (E12), #8096.

Forget, F., Pierrehumbert, R.T., 1997. Warming early Mars with carbon dioxide clouds that scatter infrared radiation. *Science* **278**, 1273–1276.

Gellert, R., Rieder, R., Anderson, R.C., Brückner, J., Clark, B.C., Dreibus, G., Economou, T., Klingelhöfer, G., Lugmair, G.W., Ming, D.W., Squyres, S.W., d'Uston, C., Wänke, H., Yen, A., Zipfel, J., 2004. Chemistry of rocks and soils in Gusev Crater from the Alpha particle X-ray spectrometer. *Science* **305** (5685), 829–832.

Glotch, T.D., Morris, R.V., Christensen, P.R., Sharp, T.G., 2004. Effect of precursor mineralogy on the thermal infrared emission spectra of hematite: application to Martian hematite mineralization. *J. Geophys. Res.* **109** (E07003).

Goetz, W., Bertelsen, P., Binau, C.S., Gunnlaugsson, H.P., Hviid, S.F., Kinch, K.M., Madsen, D.E., Madsen, M.B., Olsen, M., Gellert, R., Klingelhöfer, G., Ming, D.W., Morris, R.V., Rieder, R., Rodionov, D.S., de Souza Jr., P.A., Schröder, C., Squyres, S.W., Wdowiak, T., Yen, A., 2005. Indication of drier periods on Mars from the chemistry and mineralogy of atmospheric dust. *Nature* **436**, 62–65.

Gooding, J.L., 1978. Chemical weathering on Mars. Thermodynamic stabilities of primary minerals (and their alteration products) from mafic igneous rocks. *Icarus* **33**, 483–513.

Goulart, A.T., Fabris, J.D., Filho, M.F.d.J., Coey, J.M.D., Costa, G.M.d., Grave, E.D., 1998. Iron oxides in a soil developed from basalt. *Clays Clay Miner.* **46** (4), 369–378.

Gunnlaugsson, H.P., Weyer, G., Helgason, Ö., 2002. Titanomaghemite in Icelandic basalt : possible clues for the strongly magnetic phase in Martian soil and dust. *Planet. Space Sci.* **50**, 157–161.

Hargraves, R.B., Collinson, D.W., Arvidson, R.E., Gates, P.M., 1979. Viking magnetic properties experiment: extended mission results. *J. Geophys. Res.* **84** (B14), 8379–8384.

Hargraves, R.B., Knudsen, J.M., Bertelsen, P., Goetz, W., Gunnlaugsson, H.P., Hviid, S.F., Madsen, M.B., Olsen, M., 2000. Magnetic enhancement on the surface of Mars? *J. Geophys. Res.* **105** (E1), 1819–1827.

Haskin, L.A., Wang, A., Jolliff, B.L., McSween Jr., H.Y., Clark, B.C., Des Marais, D.J., McLennan, S.M., Tosca, N.J., Hurowitz, J.A., Farmer, J.D., Yen, A., Squyres, S.W., Arvidson, R.E., Klingelhöfer, G., Schröder, C., de Souza Jr., P.A., Ming, D.W., Gellert, R., Zipfel, J., Brückner, J., Bell III, J.F., Herkenhoff, K., Christensen, P.R., Ruff, S., Blaney, D., Gorevan, S., Cabrol, N.A., Crumpler, L., Grant, J., Soderblom, L., 2005. Water alteration of rocks and soils on Mars at the spirit rover site in Gusev Crater. *Nature* **436**, 66–69.

Hviid, S.F., Madsen, M.B., Gunnlaugsson, H.P., Goetz, W., Knudsen, J.M., Hargraves, R.B., Smith, P., Britt, D., Dinesen, A.R., Mogensen, C.T., Olsen, M., Pedersen, C.T., Vistisen, L., 1997. Magnetic properties experiments on the Mars pathfinder lander: preliminary results. *Science* **278**, 1768–1770.

Hynek, B.M., Arvidson, R.E., Phillips, R.J., 2002. Geologic setting and origin of Terra Meridiani hematite deposit on Mars. *J. Geophys. Res.* **107** (E10), #5088.

Janzen, M.P., Nicholson, R.V., Scharer, J.M., 2000. Pyrrhotite reaction kinetics: reaction rates for oxidation by oxygen, ferric iron, and for nonoxidative dissolution. *Geochim. Cosmochim. Acta* **64** (9), 1511–1522.

Jerz, J.K., Rimstidt, J.D., 2004. Pyrite oxidation in moist air. *Geochim. Cosmochim. Acta* **68** (4), 701–714.

Kaskiala, T., 2002. Determination of oxygen solubility in aqueous sulphuric acid media. *Miner. Eng.* **15**, 853–857.

Kirkland, L.E., Herr, K.C., 2000. Spectral anomalies in the 11 and 12 μm region from the Mariner Mars 7 infrared spectrometer. *J. Geophys. Res.* **105** (E9), 22507–22515.

Klingelhöfer, G., Morris, R.V., Bernhardt, B., Schröder, S., Rodionov, D.S., de Souza Jr., P.A., Yen, A., Gellert, R., Evlanov, E.N., Zubkov, B., Foh, J., Bonnes, U., Kankeleit, E., Gütlich, P., Ming, D.W., Renz, F., Wdowiak, T., Squyres, S.W., Arvidson, R.E., 2004. Jarosite and hematite at Meridiani Planum from Opportunity's Mössbauer spectrometer. *Science* **306**, 1740–1745.

Lammer, H., Lichtenegger, H.I.M., Kolb, C., Ribas, I., Guinan, E.F., Abart, R., Bauer, S.J., 2003. Loss of water from Mars: implications for the oxidation of the soil. *Icarus* **165** (1), 9–25.

Lee, M.R., Bland, P.A., 2004. Mechanisms of weathering of meteorites recovered from hot and cold deserts and the formation of phyllosilicates. *Geochim. Cosmochim. Acta* **68** (4), 893–916.

Legrand, L., Mazerolles, L., Chaussé, A., 2004. The oxidation of carbonate green rust into ferric phases: solid-state reaction or transformation via solution. *Geochim. Cosmochim. Acta* **68** (17), 3497–3507.

Lorand, J.P., Chevrier, V., Sautter, V., 2005. Sulfide mineralogy and redox conditions in some Shergottites. *Meteorit. Planet. Sci.* **40** (8), 1257–1272.

Madden, M.E.E., Bodnar, R.J., Rimstidt, J.D., 2004. Jarosite as an indicator for water-limited weathering on Mars. *Nature* **431**, 821–823.

McKibben, M.A., Barnes, H.L., 1986. Oxidation of pyrite in low temperature acidic solutions: rate laws and surface textures. *Geochim. Cosmochim. Acta* **50** (7), 1509–1520.

McSween Jr., H.Y., Murchie, S.L., Crisp, J.A., Bridges, N.T., Anderson, R.C., Bell III, J.F., Britt, D.T., Brückner, J., Dreibus, G., Economou, T., Ghosh, A., Colombeck, M.P., Greenwood, J.P., Johnson, J.R., Moore, H.J., Morris, R.V., Parker, T.J., Rieder, R., Singer, R., Wänke, H., 1999. Chemical, multispectral, and textural constraints on the composition and origin of rocks at the Mars Pathfinder landing site. *J. Geophys. Res.* **104** (E4), 8679–8715.

Mikhlin, Y.L., Kuklinskiy, A.V., Pavlenko, N.I., Varnek, V.A., Asanov, I.P., Okotrub, A.V., Selyutin, G.E., Solovyev, L.A., 2002. Spectroscopic and XRD studies of the air degradation of acid-reacted pyrrhotites. *Geochim. Cosmochim. Acta* **66** (23), 4057–4067.

Morris, R.V., Agresti, D.G., Lauer Jr. H.V., Newcomb, J.A., Shelfer, T.D., and Murali, A.V. (1989). Evidence for pigmentary hematite on Mars based on optical, magnetic, and Mössbauer studies of superparamagnetic (nanocrystalline) hematite. *J. Geophys. Res.* **94**(B3), 2760–2778.

Morris, R.V., Golden, D.C., 1998. Goldenrod pigments and the occurence of hematite and possibly goethite in the Olympus-Amazonis region of Mars. *Icarus* **134** (1), 1–10.

Morris, R.V., Golden, D.C., Bell III, J.F., Shelfer, T.D., Scheinost, A.C., Hinman, N.W., Furniss, G., Mertzman, S.A., Bishop, J.L., Ming, D.W., Allen, C.C., Britt, T., 2000. Mineralogy, composition, and alteration of Mars pathfinder rocks and soils: evidence from multispectral, elemental, and magnetic data on terrestrial analogue, SNC meteorite, and Pathfinder samples. *J. Geophys. Res.* **105** (E1), 1757–1817.

Morris, R.V., Golden, D.C., Shelfer, T.D., Lauer Jr., H.V., 1998. Lepidocrocite to maghemite to hematite : a pathway to magnetic and hematitic Martian soil. *Meteorit. Planet. Sci.* **33**, 743–751.

Morris, R.V., Klingelhöfer, G., Bernhardt, B., Schröder, C., Rodionov, D.S., de Souza Jr., P.A., Yen, A., Gellert, R., Evlanov, E.N., Foh, J., Kankeleit, E., Gütlich, P., Ming, D.W., Renz, F., Wdowiak, T., Squyres, S.W., Arvidson, R.E., 2004. Mineralogy at Gusev Crater from the Mössbauer spectrometer on the Spirit Rover. *Science* **305** (5685), 833–836.

Moses, C.O., Nordstrom, D.K., Herman, J.S., Mills, A.L., 1987. Aqueous pyrite oxidation by dissolved oxygen and by ferric ion. *Geochim. Cosmochim. Acta* **51** (6), 1561–1571.

Mycroft, J.R., Nesbitt, H.W., Pratt, A.R., 1995. X-ray photoelectron and Auger electron spectroscopy of air-oxidized pyrrhotite: distribution of oxidized species with depth. *Geochim. Cosmochim. Acta* **59** (4), 721–733.

Newsom, H.E., Hagerty, J.J., 1997. Chemical components of the Martian soil: melt degassing, hydrotermal alteration and chondritic debris. *J. Geophys. Res.* **102** (E8), 19345–19355.

Newsom, H.E., Hagerty, J.J., Goff, F., 1999. Mixed hydrothermal fluids and the origin of the Martian soil. *J. Geophys. Res.* **104** (E4), 8717–8728.

Nicholson, R.V., Gillham, R.W., Reardon, E.J., 1990. Pyrite oxidation in carbonate-buffered solution: 2. Rate control by oxide coatings. *Geochim. Cosmochim. Acta* **54**, 395–402.

Oyama, V.I., Berdahl, B.J., Woeller, F., Lehwalt, M., 1978. The chemical activities of the Viking biology experiments and the arguments for the presence of superoxides, peroxides, gamma-Fe2O3 and carbon suboxide polymer in the Martian soil. *Life Sci. Space Res.* **16**, 3–8.

Phillips, R.J., Zuber, M.T., Salomon, S.C., Golombek, M.P., Jakosky, B.M., Banerdt, W.B., Smith, D.E., Williams, R.M.E., Hynek, B.M., Aharonson, O., Hauck II, S.A., 2001. Ancient geodynamic and global-scale hydrology on Mars. *Science* **291**, 2587–2591.

Pollack, J.B., Kasting, J.F., Richardson, S.M., Poliakoff, K., 1987. The case for a wet, warm climate on early Mars. *Icarus* **71** (2), 203–224.

Posey-Dowty, J., Moskowitz, B., Crerar, D., Hargraves, R., Tanenbaum, L., Dowty, E., 1986. Iron oxide and hydroxide precipitation from ferrous solutions and its relevance to Martian surface mineralogy. *Icarus* **66**, 105–116.

Postawko, S.E., Kuhn, W.R., 1986. Effect of the greenhouse gases (CO_2, H_2O, SO_2) on Martian paleoclimate. In: Proceedings of the sixteenth Lunar and Planetary Science Conference, Part II. *J. Geophys. Res.* **91**(B4), D431–D438.

Poulet, F., Bibring, J.-P., Mustard, J.F., Gendrin, A., Mangold, N., Langevin, Y., Arvidson, R.E., Gondet, B., Gomez, C., OMEGA Team., 2005. Phyllosilicates on Mars and Implications for the Early Mars History. *Nature* **481**, 623–627.

Pratt, A.R., Nesbitt, H.W., 1997. Pyrrhotite leaching in acid mixtures of HCl and H_2SO_4. *Am. J. Sci.* **297**, 807–820.

Refait, P., Géhin, A., Abdelmoula, M., Génin, J.-M.R., 2003. Coprecipitation thermodynamics of iron(II-III) hydroxysulphate green rust from Fe(II) and Fe(III) salts. *Corros. Sci.* **45**, 659–676.

Rochette, P., Lorand, J.-P., Fillion, G., Sautter, V., 2001. Pyrrhotite and the remanent magnetization of SNC meteorites : a changing perspective on Martian magnetism. *Earth Planet. Sci. Lett.*, 1–12.

Savoye, S., Legrand, L., Sagon, G., Lecomte, S., Chausse, A., Messina, R., Toulhoat, P., 2001. Experimental investigations on iron corrosion products in bicarbonate/carbonate-containing solutions at 90 °C. *Corros. Sci.* **43**, 2049–2064.

Schwertmann, U., 1985. The effect of pedogenic environment on iron oxide minerals. *Adv. Soil Sci.* **1**, 171–200.

Schwertmann, U., Cornell, R.M., 1991. *Iron oxides in the laboratory: Preparation and characterization*. VCH Publishers, Inc., New York, NY, USA.

Schwertmann, U., Friedl, J., Stanjek, H., 1999. From Fe(III) ions to ferrihydrite and then to hematite. *J. Colloid Interface Sci.* **209**, 215–223.

Squyres, S.W., Gotzinger, J.P., Arvidson, R.E., Bell III, J.F., Calvin, W., Christensen, P.R., Clark, B.C., Crisp, J.A., Farrand, W.H., Herkenhoff, K.E., Johnson, J.R., Klingelhöfer, G., Knoll, A.H., McLennan, S.M., McSween Jr., H.Y., Morris, R.V., Rice Jr., J.W., Rieder, R., Soderblom, L.A., 2004. In situ evidence for an ancient aqueous environment at Meridiani Planum, Mars. *Science* **306**, 1709–1714.

Tardy, Y., Bardossy, G., Nahon, D., 1988. Fluctuations de l'activité de l'eau et successions de minéraux hydratés et déshydratés au sein des profils latéitiques ferrugineux et bauxitiques. *C.R. Acad. Sci. Paris II* **307**, 753–759.

Tardy, Y., Nahon, D., 1985. Geochemistry of laterites, stability of Al-goethite, Al-hematite and Fe^{3+} kaolinites in bauxites and ferricretes. *Am. J. Sci.* **285**, 865–903.

Torrent, J., Guzman, R., Parra, M.A., 1982. Influence of relative humidity on the crystallization of Fe(III) oxides from ferrihydrite. *Clays Clay Miner.* **30** (5), 337–340.

Wen, C.Y., 1968. Noncatalytic heterogeneous solid fluid reaction models. *Ind. Eng. Chem.* **60** (9), 34–54.

Yen, A.S., Gellert, R., Schröder, C., Morris, R.V., Bell III, J.F., Knudson, A.T., Clark, B.C., Ming, D.W., Crisp, J.A., Arvidson, R.E., Blaney, D., Brückner, J., Christensen, P.R., DesMarais, D.J., de Souza Jr., P.A., Economou, T.E., Ghosh, A., Hahn, B.C., Herkenhoff, K.E., Haskin, L.A., Hurowitz, J.A., Joliff, B.L., Johnson, J.R., Klingelhöfer, G., Madsen, M.B., McLennan, S.M., McSween Jr., H.Y., Richter, L., Rieder, R., Rodionov, D., Soderblom, L., Squyres, S.W., Tosca, N.J., Wang, A., Wyatt, M., Zipfel, J., 2005. An integrated view of the chemistry and mineralogy of Martian soils. *Nature* **436**, 49–54.

Yen, A.S., Kim, S.S., Hecht, M.H., Frant, M.S., Murray, B., 2000. Evidence that the reactivity of the Martian soils is due to superoxide ions. *Science* **289** (5486), 1909–1912.